Nanoscale

MINIREVIEW

View Article Online
View Journal | View Issue

Cite this: *Nanoscale*, 2024, **16**, 5903

Recent advances in the role of interfacial liquids in electrochemical reactions

Rani Baidoun, [a] Gexu Liu[b] and Dohyung Kim *[a]

The interfacial liquid, situated in proximity to an electrode or catalyst, plays a vital role in determining the activity and selectivity of crucial electrochemical reactions, including hydrogen evolution, oxygen evolution/reduction, and carbon dioxide reduction. Thus, there has been a growing interest in better understanding the behavior and the catalytic effect of its constituents. This minireview examines the impact of interfacial liquids on electrocatalysis, specifically the effects of water molecules and ionic species present at the interface. How the structure of interfacial water, distinct from the bulk, can affect charge transfer kinetics and transport of species is presented. Furthermore, how cations and anions (de)stabilize intermediates and transition states, compete for adsorption with reaction species, and act as local environment modifiers including pH and the surrounding solvent structure are described in detail. These effects can promote or inhibit reactions in various ways. This comprehensive exploration provides valuable insights for tailoring interfacial liquids to optimize electrochemical reactions.

Received 30th November 2023,
Accepted 27th February 2024

DOI: 10.1039/d3nr06092f

rsc.li/nanoscale

1. Introduction

The field of electrocatalysis has so far greatly advanced with a focus on the design and engineering of materials that would act as efficient catalysts for various important applications.[1–8] While further efforts are needed to improve the activity and stability of catalyst materials and find more earth-abundant and cost-effective alternatives, there also has been growing recognition of the importance of the interfacial liquid found at the catalyst-electrolyte interface for electrochemical applications.[6,9] The interfacial liquid, which includes species such as cations, anions, water, and other compounds found in the electric double layer (EDL) and near the surface, is considered an integral part of (photo) electrochemical systems.[9–12]

It has been demonstrated that these species within the liquid interface have an undeniable impact on important electrocatalytic reactions such as the hydrogen evolution/oxidation reactions (HER/HOR), oxygen evolution/reduction reactions (OER/ORR), and carbon dioxide reduction reaction (CO_2RR).[13–16] These reactions are key to promoting sustainable energy conversion and storage as well as reducing and reversing greenhouse gas emissions by generating value-added pro-

[a]*Department of Chemical and Biomolecular Engineering, University of Pennsylvania, Philadelphia, PA 19104, USA. E-mail: dohyungk@seas.upenn.edu*
[b]*Department of Materials Science and Engineering, University of Pennsylvania, Philadelphia, PA 19104, USA*

Rani Baidoun

Rani Baidoun obtained his BS degree in Chemical and Biomolecular Engineering from Lehigh university. Currently, he is a second year Ph.D. candidate in the Chemical and Biomolecular Engineering Department of the University of Pennsylvania. His research focuses on interfacial microenvironments at the electrode/electrolyte interface as well as electrochemical bond cleavage.

Gexu Liu

Gexu Liu obtained her BS degree in Material and Nano Science from University of Waterloo and BEng degree in Material Science and Technology from Beijing Jiaotong University. Currently, she is a master's student at University of Pennsylvania, focusing on interfacial liquids and their impact on electrochemical reactions.

ducts with renewables.[6,17,18] In electrochemical systems, these reactions take place as follows:

$$\mathrm{HER/HOR}: 2H^+ + 2e^- \rightleftarrows H_2$$

$$\mathrm{OER/ORR}: 2H_2O \rightleftarrows O_2 + 4H^+ + 4e^-$$

$$CO_2\mathrm{RR}: CO_2 + 2H^+ + 2e^- \rightarrow CO + H_2O$$

$$2CO_2 + 12H^+ + 12e^- \rightarrow C_2H_4 + 4H_2O$$

They often involve a large number of elementary steps. Furthermore, for the ORR and CO_2RR, there exist multiple reaction pathways, such as the $2e^-$ pathway for ORR to produce H_2O_2 and a multielectron reduction pathway for CO_2 to produce hydrocarbons and oxygenates. For a better understanding of all the details regarding the mechanisms of those reactions as well as the catalyst design considerations, readers are encouraged to go over other excellent perspectives and reviews published previously.[13–16,19–21]

This minireview focuses on how the interfacial liquid affects the rates and selectivity of these reactions. Understanding the behavior of water molecules at the solid–liquid interface, distinct from the bulk, is crucial for water-splitting electrochemistry. Ionic species are critical components of the EDL that form against a charged solid and their presence near the active sites can significantly facilitate or inhibit reactions in numerous ways that include intermediate (de)stabilization,[22,23] local environment modification (*e.g.*, pH, solvent structure),[24,25] and active site modification (*e.g.*, electronic structure, accessibility).[26] While the recognition of such catalytic effects at electrochemical interfaces is not new,[9,27] recent advances in experimental and theoretical approaches have significantly enhanced our understanding of the impacts of interfacial liquids on electrochemical reactions. This minireview highlights the latest findings in this evolving field. Advancements in both catalyst synthesis and the manipulation of interfacial liquid effects are poised to elevate the efficiencies of electrochemical reactions to unprecedented levels.

In this minireview, we delve into the latest advances and current insights in three distinct sections, offering a detailed overview of the electrocatalytic impacts of structured interfacial water, solvated and desolvated cations, and specifically and non-specifically adsorbing anions, as summarized in Table 1. Due to the growing importance of interfacial liquids in electrocatalytic reactions, there have been recent reviews particularly focused on the cation effects in CO_2 electroreduction.[28–31] Given the ubiquity of interfacial liquids and their far-reaching implications in various essential reactions, our objective is to offer a more thorough examination of all species within the interfacial liquid. We describe their general effects and diverse influences on activity and selectivity across different reactions. Regarding the mechanisms, we present varying perspectives, many of which are actively under investigation. This minireview is meticulously curated to provide a comprehensive overview of our latest understanding in this area and propose avenues for future research to advance our knowledge.

Dohyung Kim

Dohyung Kim is an Assistant Professor in the Department of Chemical and Biomolecular Engineering at the University of Pennsylvania. He received his B.S. in Materials Science and Engineering from Seoul National University in 2012 and a Ph.D. in Materials Science and Engineering from the University of California, Berkeley in 2018. Before joining Penn in 2022, he was a postdoctoral scholar at the Department of Chemical Engineering, Stanford University. His research focuses on gaining fundamental insights into electrochemical processes occurring at solid–liquid interfaces and applying such knowledge to various areas of energy, chemicals, materials, and the environment.

2. Structured water at the interface

In most electrochemical systems containing aqueous electrolytes, water is the predominant species. The arrangement and orientation of water molecules within the interfacial liquid have been shown to have a significant impact on various electrochemical reactions, such as the HER and CO_2RR.[32] Therefore, gaining insights into the dynamic behavior of interfacial water as well as its overall structure by the hydrogen bonding network is vital in order to better control these electrochemical reactions. In this section, we elucidate the relationship between the structure of the interfacial water and the activity and selectivity of HER and CO_2RR, while also delving into the underlying molecular mechanisms.

2.1. Hydrogen evolution reaction

Efforts to understand the impact of water molecules on HER have primarily focused on alkaline media systems, where the rates are sluggish.[32,33] It has been suggested that the interfacial microenvironment, specifically the structure of water molecules, serves as an important descriptor of HER kinetics in alkaline media.[34] In recent discourse, two primary viewpoints have emerged concerning the mechanism by which the structure of interfacial water molecules influences the rates of HER. The first view posits that the hydrogen-bonded interfacial water may introduce structural rigidity difficult to accommodate HER intermediates *via* reorganization and slow the kinetics. On the other hand, there have been works emphasizing the connectivity of the hydrogen-bonded interfacial water network that facilitates the transfer of proton/hydroxides and therefore increases HER activity.

Rigidity of structured water and its kinetic effect. With regards to the first view, Ledezma-Yanez *et al.* explain that the interfacial reorganization of water molecules and their interaction with intermediate species govern HER kinetics.[33] The

Table 1 A summary of all the effects of different interfacial species on the important reactions discussed in this review

Reactions	Interfacial liquid components	Effects
HER	Water molecules	• More rigid water structures lead to higher kinetic barriers due to higher reorganization energy requirements • Structured water facilitates H/OH transport leading to higher HER activities
	Cations	• Smaller alkali metal cations lead to higher HER activity on Pt-group metals and lower HER activity on coinage metals • Cations stabilizing HER transition states either directly or indirectly (*e.g.*, *via* adsorbed OH) • Cations can alter the water reorganization energy
OER/ORR	Cations	• Larger alkali metal cations lead to increase in OER • Cations can stabilize or destabilize key OER and ORR intermediates affecting reaction rates • Larger alkali metal cations disrupt water networks which facilitates the rearrangement of water molecules during with charge transfer • Cations also influence the local pH with higher pH values leading to higher OER activities • Cations influence the formation of catalytically active phases under operation for OER
	Anions	• Anions exhibiting poisoning effects and decreasing ORR rates
CO_2RR/CORR	Water molecules	• Hydrophobic environments and breakage of water networks hinder HER and favor CO_2RR • Stabilize key reaction intermediates *via* H-bond interactions
	Cations	• Larger alkali metal cations increase CO_2RR/CORR rates through local electric field modulation and direct intermediate stabilization • Alkali metal cations buffer the local pH, therefore controlling the reactant concentration (*i.e.*, CO_2) near the surface
	Anions	• Halides donate partial negative charge to the catalyst surface enhancing the interaction with reaction intermediates • Supporting electrolyte anions, such as bicarbonate, also function as an additional proton and CO_2 source

authors show that with increasing pH the overpotential required for HER increases which is a behavior that cannot be described by the change in the hydrogen binding energy (HBE) (Fig. 1A).[33] Through electrochemical impedance spectroscopy (EIS), they demonstrate that charge transfer resistance for the hydrogen underpotential deposition (H-UPD) increases with

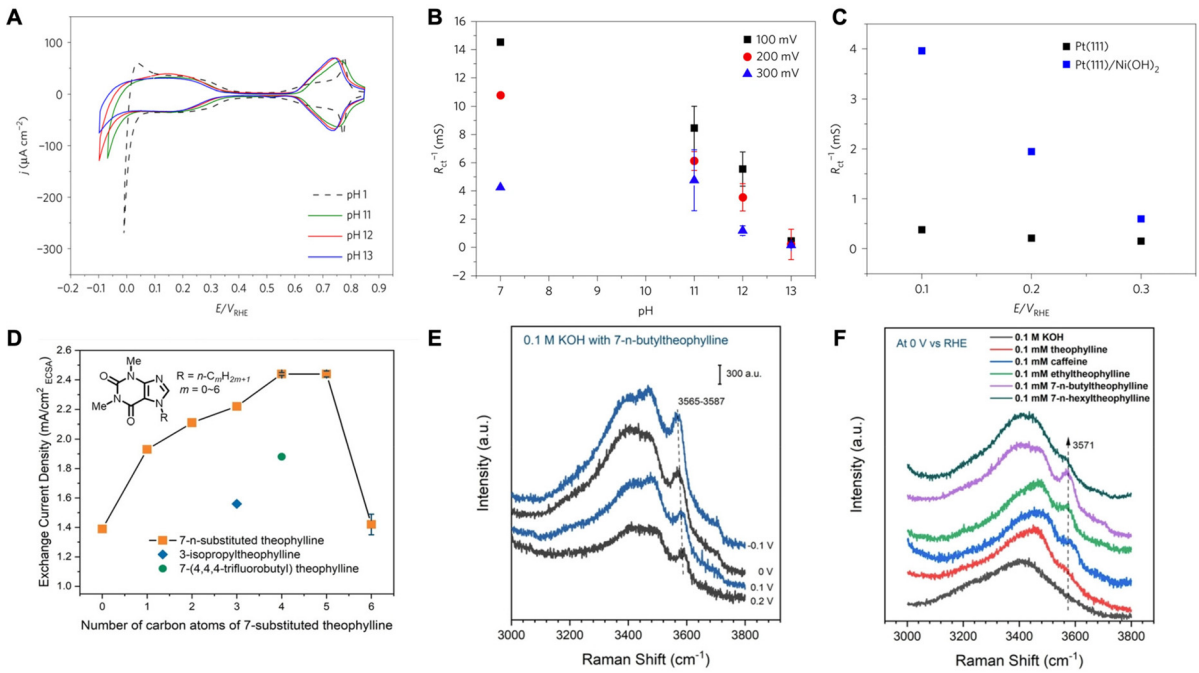

Fig. 1 (A) Comparison of cyclic voltammograms for Pt(111) at different pH values. (B) Inverse of charge transfer resistance for hydrogen adsorption as a function of solution pH. (C) The inverse of charge transfer resistance for hydrogen adsorption as a function of potential for Pt(111) and $Ni(OH)_2$ decorated Pt(111). Reproduced from ref. 33 with permission from Springer Nature, copyright 2017. (D) HER/HOR activities on polycrystalline (pc) Pt in H_2-saturated 0.1 M KOH with 0.1 mM theophylline derivatives. (E) *In situ* SHINERS of interfacial water on a Pt(pc) electrode in 0.1 M KOH with 0.1 mM 7-*n*-butyltheophylline at −0.1 to 0.2 V. (F) *In situ* SHINERS of interfacial water on a Pt(pc) electrode in 0.1 M KOH with 0.1 mM various theophylline derivatives at 0 V. Reproduced from ref. 35 with permission from John Wiley and Sons, copyright 2022.

pH (Fig. 1B). Tafel analysis also shows that an increase in pH makes the H adsorption step sluggish. The authors attribute this behavior to the interfacial water structure rigidity. Near the potential of zero free charge (pzfc), water is not as rigid and is easy to reorganize. However, at potentials further from the pzfc (*i.e.*, strong electric field present at the electrode/electrolyte interface), water becomes rigid and difficult to reorganize. In alkaline media, Pt exhibits a high pzfc compared to that in acidic conditions and at the potential range for H-UPD and HER a more rigid interfacial water structure exists leading to a large reorganization energy to accommodate OH^- released during charge transfer slowing down H-UPD and HER.

They went on to further show that by manipulating the pzfc and the resulting interfacial water rigidity, HER kinetics in alkaline media can be improved. Through laser-induced temperature-jump measurements, it was found the electric field strength decreases due to a negative shift in the pzfc when Ni$(OH)_2$ is adsorbed on Pt. This brings the H-UPD and HER potential region closer to the pzfc and makes the interfacial water less rigid resulting in the improved kinetics for Pt/Ni$(OH)_2$ (Fig. 1C). These results highlight the significance of interfacial water structure on the kinetics of HER.

In another work, Intikhab *et al.* studied the effects of double-layer dopants such as caffeine on the HER/HOR reactions in alkaline media.[36] They demonstrated that both HER and HOR rates increased by 5-fold on a Pt(111) surface in alkaline media in the presence of caffeine as the double layer dopant. They also demonstrated an increase in HER/HOR rates on other Pt single crystals as well as polycrystalline surfaces and nanoscale surfaces such as Pt/C. For instance, on Pt(pc), the exchange current densities increased from 0.30 mA cm^{-2} to 0.86 mA cm^{-2}, whereas on Pt(110), the exchange current densities increased from 1.03 mA cm^{-2} to 2.21 mA cm^{-2}. Furthermore, the authors demonstrate that caffeine adsorbs on the surface of the catalyst as evidenced by H-UPD region suppression and remains stable up to potentials of 1.0 V *vs.* RHE. The authors then studied the effects of caffeine in acidic environments (pH = 1) where they demonstrated that HER/HOR kinetics are hindered rather than enhanced. They explain that because the electric field in the H-UPD region is stronger in alkaline media than in acidic media, the caffeine molecule disrupts this electric field and therefore lowers the barrier for water reorganization. In acidic media however, since the electric field is weak in the H-UPD region (close to the pzc), water reorganization does not play a role in impacting the rates of these reactions, and therefore caffeine only acts as a hindrance through site blocking.

Based on a similar school of thought, Zhao and coworkers explored the enhancement of HER/HOR by introducing caffeine-derivative organic compounds that act as interfacial water structure disruptors.[35] They determined that 7-*n*-butyltheophylline increased the HER activity the most by inducing surface hydrophobicity on Pt (Fig. 1D). Through *in situ* surface enhanced infrared absorption spectroscopy (SEIRAS), they determined that 7-*n*-butyltheophylline is strongly bound to the Pt surface with an adsorption energy comparable to CO adsorption on Pt. Due to its interfacial specificity, shell-isolated nanoparticle enhanced Raman spectroscopy (SHINERS) was employed to understand the interfacial water structure in different coordination environments. It is observed that a sharp band appears upon adsorption of 7-*n*-butyltheophylline. This band corresponds to weakly H-bonded water molecules. The band red shifts as well as increases in intensity with decreasing potential suggesting the presence of these water molecules in the immediate proximity of the electrode surface, especially in the presence of 7-*n*-butyltheophylline than other derivatives (Fig. 1E and F). The authors propose that alkyl groups on adsorbed 7-substituted theophylline act as structure breakers of interfacial water by disrupting their H-bond network, therefore decreasing the activation energy of the HOR/HER. The weakening of H-bonds within interfacial water molecules makes it less energetically costly to change their configuration to stabilize the intermediates of the HER/HOR reaction. This H-bonding network disruption by alkyl chain adsorbates is local and only reactions occurring on unoccupied Pt sites close to the adsorbates would be impacted.

Rebollar *et al.* further studied caffeinated systems and the consequences of the HER/HOR reactions on Pt surfaces.[37] The authors demonstrated once more that the presence of caffeine hinders HER/HOR in acidic media while boosting the reaction in alkaline media. The authors attributed this change in activity to the pzfc shift and its effects. The pzfc shifted to negative values in the presence of caffeine indicating that in alkaline media caffeine disrupts the electric field allowing for an enhancement in HER/HOR. Furthermore, while the pzfc was very close to the RHE in a caffeine-containing base, it actually shifted further away from the RHE in a caffeine-containing acid, also explaining the slower kinetics in acid in the presence of caffeine. The authors also demonstrated that the presence of caffeine enhanced alkaline HER/HOR regardless of the pH and inhibited HER/HOR in acidic media. Overall, they were able to confirm the pH effects on HER/HOR that may be associated with how close the pzfc is to the RHE potential that reduces the kinetic barriers associated with solvent dynamics suggested by Ledezma-Yanez *et al.*[33] However, they also suggest that there might be other mechanistic reasons to the widely varying degree of HER/HOR kinetics across different pHs and the enhancement in alkaline media caused by adsorbed molecules, such as the caffeine, as kinetic isotope experiments show that solvent dynamics are fast in acid and slow in base regardless of the pzfc shift by the adsorbed caffeine.

H transport facilitated by a structured water network. From another perspective, Wang *et al.* claim that a more ordered interfacial water layer is beneficial to HER.[38] The authors developed a framework to correlate the effects of cations and interfacial water on Pd HER activity in a pH 11 $NaClO_4$ solution. In general, they demonstrate the importance of Na^+ cations which supply the surface of the catalyst with ordered water molecules and therefore increase the activity of HER (Fig. 2A). They utilize a combination of SHINERS and *ab initio* molecular dynamics (AIMD) simulations to demonstrate the

dynamically changing interfacial water structure. SHINERS revealed a band at 550 cm^{-1} that began to emerge around a potential of −0.11 V *vs.* RHE and increased in intensity with increasing negative potential indicating the formation of an ordered water structure with a larger negative potential (Fig. 2B). Furthermore, Gaussian fitting of the Raman spectra shows that due to the electrostatic effect of cation migration towards the surface, there was an increase in the Na^+ ion hydrated water population. The vibrational frequency of adsorbates was found to vary with electrode potential due to the Stark effect. Steeper Stark slopes show that Na^+ ion hydrated water ($Na{\cdot}H_2O$) is more sensitive than hydrogen-bonded water at any coordination. Further AIMD simulations demonstrate that, in Na^+ containing electrolyte with decreasing potential (*i.e.*, more negative potentials), the Pd–H bond length decreased along with the Fermi level of Pd approaching the empty antibonding orbital of water. The decrease in Pd–H length by the Na^+ promotes water dissociation, charge transfer efficiency, and HER activity (Fig. 2C).

In another work by Sun and coworkers, it was demonstrated that the addition of *N*-methylimidazoles at the platinum–water interface promotes HER rates by facilitating the diffusion of hydroxides through an ordered interfacial water structure.[39] They propose that HER/HOR kinetics of Pt in acid and base media are dependent on the diffusion of protons and hydroxides, respectively, through the H-bonding network of inter-

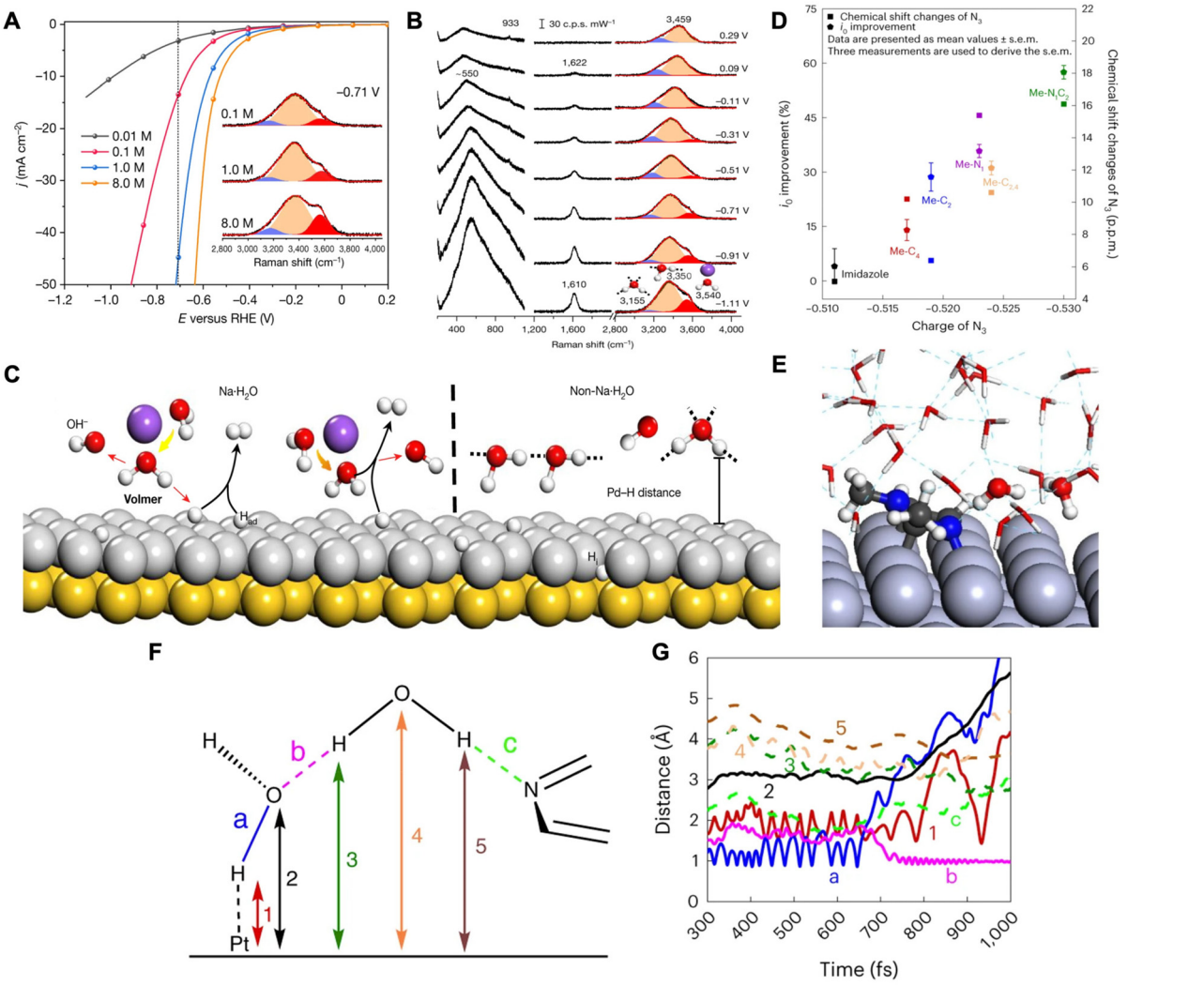

Fig. 2 (A) HER profiles for solutions with different Na^+ cations and Raman spectra for O–H stretching modes (inset). (B) *In situ* Raman spectra of interfacial water on a Pd(111) electrode in a 0.1 M $NaClO_4$ electrolyte of pH 11. Gaussian fitting of three O–H stretching modes for each spectrum is shown in blue, orange, and red. (C) Schematic for the interfacial water dissociation on an Au(111) coated with Pd(111) surface. Reproduced from ref. 38 with permission from Springer Nature, copyright 2021. (D) Improvements in the i_0 (left *y*-axis) and $^{14}N_3/^{15}N_3$ chemical shift changes (right *y*-axis) of *N*-methylimidazoles between two different media as a function of N_3 charge. Note: N_3 charge was calculated using DFT. (E) Atomic configuration of an equilibrated H_2O–Pt(100) system including Me–N_1C_2 in alkaline medium. (F) Schematic of an interfacial water dimer composed of H_2O(H-down)^{1st} and an N_3 of Me–N_1C_2 bonded with an H_2O(H-down)^{2nd}. (G) Time evolution of bond distances during the Volmer step at the H_2O–Pt(100) interface with Me–N_1C_2 in alkaline medium. Reproduced from ref. 39 with permission from Springer Nature, copyright 2023.

facial water by the Grotthuss mechanism. The Grotthuss mechanism involves proton migration within the H-bonding network of water, where a proton jumps from one stationary oxygen atom to a neighboring oxygen atom through the cleavage and formation of bonds.[40,41] The authors performed rotating disk electrode (RDE), density functional theory (DFT), and ^{14}N and ^{15}N Nuclear Magnetic Resonance (NMR) studies in order to understand the effects of *N*-methylimidazoles on HER. From RDE measurements, a trend was found that the greater the number of methyl groups, the higher the exchange current density leading to higher HER/HOR rates. With DFT determining the partial charges of *N*-methylimidazole combined with RDE and NMR results, they show that Me–N_1C_2 (1,2-dimethylimidazole) exhibits the most negative N_3 (pyridinic nitrogen of *N*-methylimidazole) and the strongest N_3–H_2O bond leading to the highest exchange current density (i_0) (Fig. 2D). Furthermore, the authors conducted a combination of *in situ* attenuated total reflectance surface-enhanced infrared reflection absorption spectroscopy (ATR-SEIRAS) and AIMD to understand *N*-methylimidazole's interaction with interfacial water. *In situ* ATR-SEIRAS spectra for Me–N_1C_2-free electrolyte demonstrate water reorganization from the H-up, proton donor position to the H-down, proton acceptor position due to the negatively charged Pt surface. Furthermore, when adding Me–N_1C_2, the spectra do not exhibit changes indicating that the strong H-bonded interfacial water near the Pt remains intact.

AIMD simulations were conducted on the Pt(100)–water interface with and without Me–N_1C_2. Without the Me–N_1C_2, the water molecules closest to the Pt (first layer) were organized in the H-down orientation (denoted as: $H_2O(H\text{-down})^{1st}$) due to the negatively charged surface and the O–H dipole. These $H_2O(H\text{-down})^{1st}$ (proton acceptors) form H-bonds with $H_2O(H\text{-down})^{2nd}$ (proton donors) and therefore construct the interfacial H-bond network. When Me–N_1C_2 was introduced, the energetically favorable binding configuration was the parallel binding of the imidazole ring. In this configuration, the $H_2O(H\text{-down})^{2nd}$ is an H-bond donor to both the $H_2O(H\text{-down})^{1st}$ and the N_3 (Fig. 2E). Metadynamic simulations show that, as potential is applied in the absence of Me–N_1C_2, the $H_2O(H\text{-down})^{1st}$ adsorbs to the surface and dissociates and the generated hydroxide is chemisorbed onto the surface. When Me–N_1C_2 is introduced, the hydroxide that is generated is hydrogenated by the $H_2O(H\text{-down})^{2nd}$ that is bound to Me–N_1C_2. This replenishes the $H_2O(H\text{-down})^{1st}$ as indicated by a decrease in the H-bond length between $H_2O(H\text{-down})^{1st}$ and $H_2O(H\text{-down})^{2nd}$ (Fig. 2F and 'b' in 2G). Thereafter, the hydroxide continues diffusing through the Grotthuss mechanism. The catalytic enhancement observed with Me–N_1C_2 was attributed to its ability to bring the second layer of water molecules closer to the surface through its interactions, thus facilitating hydroxide diffusion within the water network.

There have been other views on the effect of cations on the H-bonding network at the electrode–electrolyte interface. Li *et al.* performed AIMD simulations to illustrate the differences between the structure of the EDL in acidic and alkaline media.[34] They found that the closest ion plane (CIP) in alkaline media is closer to the electrode surface and has a higher cation concentration than in acidic media. The crowded cations in alkaline media lose their solvation shell and cause a water gap above the CIP. This gap, in turn, disrupts the H-bond network and therefore disrupts the proton "highway" decreasing HER activity. Theoretical vibrational density of states (VDOS) calculations and *in situ* SEIRAS further reveal the scarcity of H-bond networks in the gap region. The authors conclude that the discontinuity in the H-bonding network in alkaline media due to cation presence plays a large role in the sluggishness of HER. Furthermore, the addition of a more oxophillic Ru to the Pt surface promotes OH adsorption which decreases the water gap and facilitates H-bonding connectivity thereby improving HER activity.

A follow-up work by Su *et al.* explored the pH effect of HER/HOR on various metal catalysts.[42] Instead of a decrease in HER/HOR rates with increasing pH, they observed an inflection point where the rates of HER/HOR begin to increase once more after a specific pH. Using a triple-path microkinetic model, it was revealed that the formation of OH_{ad} promotes the HOR/HER kinetics by improving the H-bond network in the EDL instead of decreasing intermediate reaction energy barriers. The authors claim that since the electrode is more negatively charged in HER/HOR potential regions at higher pH (*i.e.*, higher pzfc at higher pH), the surface becomes crowded with cations which in turn weakens the H-bonding between the water molecules close to the surface and the ones further away in the EDL. The presence of OH_{ad}, however, reduces the strength of cation–water interactions due to OH_{ad}–cation interactions and regenerates some of the H-bonded water networks. This effect of OH_{ad} would be more pronounced on catalysts with stronger hydroxide binding energies and such was experimentally observed for more oxophillic catalysts.

It is evident that the structure of interfacial water critically affects the HER in diverse media and on various catalyst materials. Despite all research efforts, the precise mechanism by which interfacial water affects HER (or HOR) remains a topic of ongoing debate. More research is needed to develop a comprehensive understanding of how interfacial water molecules and their collective structure influence HER and to be able to control this environment for specific applications.

2.2. Carbon dioxide reduction

Numerous variables have been reported to affect the electrocatalytic reduction of CO_2.[43] Those include the bulk and local pH and the electrolyte composition and concentration. In this section, however, we focus on the effects of interfacial water on the CO_2RR. Typically, research efforts have focused on introducing ionic or organic additives to the electrolyte which create a hydrophobic interfacial environment. This decreases water diffusion to the catalyst and breaks down the water network hindering HER and boosting CO_2RR.[44,45] While these are the main effects of interfacial water discussed in the literature, it is also important to note that water molecules play other roles

regarding the CO_2RR, such as enhancing the stability of key intermediates.[46]

Mohandas *et al.* performed *in situ* SEIRAS experiments together with linear sweep voltammetry to reveal how organic additives such as DMF break down the water structure and the H-bonding network impeding HER, a competing reaction of CO_2RR.[44] Through a negative shift in onset potentials, the authors demonstrated the universality of DMF's role in the suppression of HER for various catalyst materials in argon-saturated electrolytes. However, in CO_2-saturated electrolytes, DMF positively shifted the onset potential for the CO_2RR and produced a CO faradaic efficiency (FE) of 94% on a polycrystalline Au electrode when 15 mol% DMF was introduced into the electrolyte. Through *in situ* SEIRAS and the deconvolution of O–H stretching bands, it was revealed that DMF accumulates at the interface which in turn modifies interfacial water structure by creating H-bonding interactions between the O and N of DMF molecules and interfacial water. The authors concluded that DMF-induced disruption in interfacial water structure as well as water repulsion from the interface are the main reason for HER inhibition and an increase in CO selectivity.

Ge and coworkers studied potential-driven dynamics of the interfacial microenvironment with quaternary ammonium cationic surfactant additives for the co-reduction of CO_2 and H_2O.[47] It was revealed through EIS phase angle measurements that the structure of these surfactants on the surface of electrodes dynamically changes with an increase in applied potential from a random distribution to a nearly ordered assembly. Furthermore, cetyltrimethylammonium bromide (CTAB) showed the highest double layer capacitance (C_{dl}) indicating that longer alkyl-chain surfactants are easier to adsorb. With CTAB as an electrolyte additive, various types of silver catalysts were tested for CO_2 reduction and all were found to gain in CO selectivity over H_2. *In situ* SEIRAS and *in situ* surface enhanced Raman spectroscopy (SERS) were utilized to probe the interfacial water structure in the system with and without CTAB. In the system with CTAB, the formation of a hydrophobic microenvironment was found. Furthermore, the presence of CTAB did not allow water molecules to reorient into the two H-down, proton acceptor, ordered structure. Finally, through molecular dynamics (MD) simulations, it was found that there are fewer water H-bonds in a system with CTAB than in a system without CTAB. The theoretical and experimental results demonstrate that these surfactants adsorbed to the surface create a highly hydrophobic–aerophilic environment which increases the selectivity of CO_2 to CO while simultaneously decreasing the reactivity of water dissociation and therefore HER activity.

Since the CO_2RR occurs in competition with the HER, most literature discusses the effect of additives from the perspective of creating a hydrophobic interfacial environment repelling water molecules and hindering HER while simultaneously bolstering CO_2RR. However, there has been limited research on how water molecules themselves could in fact promote CO_2RR. Meng *et al.* explored the effect of interfacial water molecules on the CO_2RR activity and selectivity using DFT and AIMD simulations with boron-doped bismuth catalysts (B@Bi and B_2@Bi).[46] From partial density of states (PDOS) calculations, the peaks of C 2p, O 2p, B 2p, and Bi 5d orbitals were found close to the Fermi level in aqueous electrolytes. These results indicate that water molecules exhibit promoter effects on CO_2 activation through H-bonding as well as enhance the CO_2 adsorption energy. Furthermore, it was found that the presence of water molecules affects the thermodynamic potential determining step (PDS). Boron-doped bismuth demonstrated lower overpotential requirements for the production of methane in a system that includes 30 H_2O than the gas-phase system. Similar results were also found for the production of ethylene. The authors attribute this to the H-bond interactions of water molecules with key reaction intermediates.

3. Thermodynamics and kinetics of reaction pathways influenced by cations

Alkali metal cations (AMCs) have been shown to exist in a coordinated hydrated environment within the electrolyte.[9] Many characteristics of the AMCs, such as the charge density (*i.e.* cation size) and the hydration degree and energy, have a significant effect on various electrochemical reactions such as the HER/HOR, OER/ORR, and the CO_2RR.[9] The exact mechanism by which AMCs affect these different reactions varies from reaction to reaction. Thermodynamically, AMCs alter intermediate stabilization *via* direct non-covalent and indirect electrostatic interactions.[22,23] Kinetically, AMCs alter solvent reorganization energies to facilitate fast charge transfers.[48] In this section, we describe the effects of AMCs on the reaction rates and selectivity of HER/HOR, OER/ORR, and CO_2RR, as well as their underlying mechanisms.

3.1. Hydrogen evolution reaction

General trends. AMCs have been shown to have a profound effect on the HER, especially in alkaline media. Also, there has been some consensus on the varying effects of different cation types. Xue and coworkers showed that on Pt and Ir electrodes, the HER activity in alkaline electrolytes increases with increasing hydration energy of the AMC (*i.e.*, decreasing cation size) and therefore as: $Li^+ > Na^+ > K^+ > Rb^+ > Cs^+$.[49] On the other hand, the trend was reversed for Au and Ag (*i.e.*, $Li^+ < Na^+ < K^+ < Rb^+ < Cs^+$). Similarly, Taji *et al.* demonstrated that the HER activities on Pt in alkaline media increased with decreasing AMC size in agreement with previous results.[50] They further utilized EIS to examine the influence of AMCs on the HER reaction mechanism and showed that, in Li^+-containing electrolytes, the Volmer–Heyrovsky (VH) mechanism contributes more to the overall reaction than the Volmer–Tafel (VT) mechanism. The authors conducted DFT simulations which showed that the energetics of the Volmer and Heyrovsky steps decrease with decreasing cation size while the energetics of the Tafel step remains the same. While smaller cations might boost Volmer kinetics on Pt surfaces, this argument fails to explain

the inverted trend seen on catalysts like Au. Similar results were also observed by Bender and coworkers. They demonstrated that AMCs have no effect on HER rates in acidic media and further confirmed the aforementioned trend in alkaline media for Pt-group metals (*i.e.*, Pt, Pd, and Ir) and coinage metals (*i.e.*, Cu, Ag, and Au), where the trends are opposite to each other.[51] It was proposed that cations decrease the energy barrier for water dissociation, especially for Cu, Ag, and Au catalysts whose ability to do so is limited. The inverted AMC effect trend (*i.e.*, $Li^+ < Na^+ < K^+ < Rb^+ < Cs^+$) for those metals is due to the more weakly solvated large cations being better able to approach the electrode surface.

Transition state stabilization by cations. To understand these effects, Jiao *et al.* studied the solid–liquid interfacial structure in the presence of cations specifically for Pt.[52] Using *in situ* X-ray absorption spectroscopy (XAS) coupled with *ab initio* FEFF calculations, they revealed that AMCs and hydroxides do not specifically adsorb onto the Pt surface while H_2O molecules (with the O atom pointed towards the catalyst) could specifically adsorb in the H-UPD region. They propose an interfacial structure of $Pt–H_2O\cdots[(H_2O)_x–AM^+]$ (AM = alkali metal) where the AMC weakens the $Pt–H_2O$ bond through non-covalent interactions.[52] Furthermore, they propose that the presence of the AMC promotes HER on Pt as it facilitates the removal of hydroxides in the form $OH\cdots[(H_2O)_x–AM^+]$ after the dissociation of water.

A study by Goyal *et al.* suggested that cations play a crucial role in stabilizing the transition state of the rate-determining Volmer step ($H_2O + e^- + * \rightarrow *H + OH^-$) through interactions with the dissociating water molecules ($*H–OH^{\delta}–M^+$).[53] They found that HER activity is enhanced on Au electrodes as the cation concentration increased at moderately alkaline conditions (Fig. 3A). Also, chronoamperometry studies reveal that as pH increases, the current at each overpotential also increases and Tafel slopes decrease indicating activity enhancement. They attribute this behavior to the indirect effect of increased pH leading to an increase in the near surface cation concentration as a result of the change in the local field strength. However, there is a volcano-type relationship where HER activity diminishes at very high pH and cation concentrations due to blockage of the catalyst surface (Fig. 3B). Thus, it seems that there is an optimal concentration of cations for promoting HER through the stabilization of transition state during water dissociation.

A follow-up study was conducted on Au and Pt electrodes to further elucidate the cation effect on HER.[54] Using Tafel analysis coupled with cyclic voltammetry (CV) on gold, they found that weakly hydrated cations such as K^+ increase HER rates on Au catalysts, but only at low overpotentials (*i.e.*, low local alkalinity, low pH). At higher overpotentials (*i.e.*, high near-surface AMC concentration), the AMCs become detrimental due to overcrowding at the outer Helmholtz plane (OHP) further confirming the previous trend.[53] However, with Pt electrodes, HER

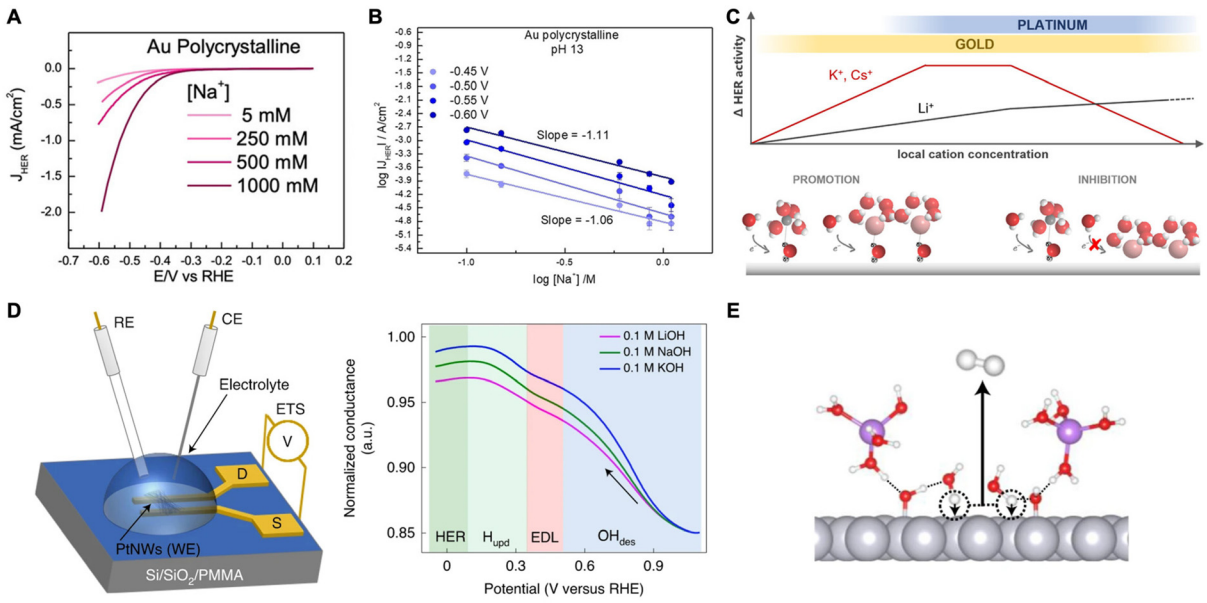

Fig. 3 (A) Cyclic voltammograms obtained for HER on a polycrystalline Au electrode in an alkaline environment (pH 11) at different Na^+ concentrations. (B) Reaction order plot of HER rates as a function of Na^+ concentration at pH 13 showing an inhibition of HER. Reproduced from ref. 53 with permission from John Wiley and Sons, copyright 2021. (C) Schematic representation illustrating the effects of local pH and AMC concentration on HER activity on Au and Pt electrodes. Reproduced from ref. 54 with permission from the American Chemical Society, copyright 2021. (D) Schematic of Pt nanowires for ETS measurements, where RE, CE, WE are the reference, counter, and working electrodes, respectively, and S and D are the source and drain terminals, respectively (left). Normalized ETS conductance plot as a function of potential showcasing the behavior of ions at the different regimes (right). (E) Schematic demonstrating the promoting effects of OH_{ads} on the alkaline Volmer step. Reproduced from ref. 55 with permission from Springer Nature, copyright 2022.

inhibition by weakly hydrated cations was observed already at low pH conditions suggesting strong Pt–AMC interactions. The authors proposed a model to explain the aforementioned inverted trend between Pt and Au (Fig. 3C). At low local pH and AMC concentration (*i.e.* a promotion regime), weakly hydrated cations better stabilize the transition state of water dissociation. However, these cations tend to interact with the surface more which then turns their promoting effects into hindering ones at higher local pH and AMC concentrations. In the inhibition regime, a negative reaction order is observed with increased cation concentration. Such is the case for Au. However, for Pt which interacts more strongly with cations, HER occurs mostly in the inhibition regime where strongly hydrated Li^+ is favored over weakly hydrated K^+ or Cs^+.

Indirect cation effect *via* hydroxyl groups. It has also been shown that cations could affect the rates of HER indirectly through the adsorption of hydroxyl groups on the catalyst surface. Chen *et al.* studied a system containing stepped sites on Pt(553).[56] They observed that AMCs co-adsorb along the step and weaken the adsorption of hydroxides causing a positive shift in the H-UPD potential of the step-related peak on Pt (553). Utilizing CV and DFT, they show that the shift is more pronounced with larger alkali cations which tend to destabilize the OH_{ads} stronger than smaller alkali cations. They also claim that as the pH increases, the PZC shifts to more positive values on the RHE scale, and therefore the step-associated peak exhibits a non-Nernstian shift with a pH dependence as well as a cation identity dependence.

In another study, Shah *et al.* utilized a combination of EIS and electrical transport spectroscopy (ETS) to study the effect of near-surface AMCs on HER rates on Pt catalysts in alkaline media.[55] As stated previously, the authors show that the smaller cations better stabilize the adsorbed hydroxide species in the H-UPD region favoring high OH_{ad} coverage on the Pt surface. Moreover, due to the high polarity of OH_{ad}, water dissociation is easier to occur, therefore boosting the Volmer-step kinetics and HER activity. From ETS analysis, they concluded that the lowest conductance was at the OH_{ad} regime due to the strongly bonded OH on the Pt surface reducing the conductance of Pt nanowires (Fig. 3D). As the potential was scanned negative, the conductance increased monotonically, first due to the replacement of OH on the surface with water molecules (EDL regime) and thereafter the replacement of water molecules and residual OH molecules with adsorbed hydrogen (H-UPD regime). Eventually, conductance levels off due to the saturation of the electrode surface with H_{ads} in the HER region. This trend was observed for all three different electrolytes with different AMCs (Li^+, Na^+, and K^+). However, the one with Li^+ showed the least increase in conductance indicating that solvated Li^+ stabilizes the OH adsorbates more than other cations. The authors further utilized DFT and AIMD simulations to confirm this trend, together with capacitance measurements that exhibit values following $Li^+ > Na^+ > K^+$ at the H_{UPD} and HER regime related to the remaining adsorbed OH. Furthermore, it was shown that adsorbed hydroxides act as H-bond acceptors/donors and therefore stabilize the near-surface water molecules decreasing their barrier for dissociation (Fig. 3E). These results indicate that HER activity is dependent on the dissociation of water and the trend of $Li^+ > Na^+ > K^+$ is due to AMC's influence on the amount of adsorbed hydroxides on Pt.

Cation acidity and multivalent cations. Monteiro and coworkers studied the effect of various cations on HER rates on a polycrystalline Au electrode at a pH of 3.[24] Through their work, they show that while cation identity does not affect proton reduction in acidic media, when the near-surface region becomes basic at high overpotentials, HER activity is the highest with trivalent cations and Be^{2+}. This is due to the hydrolysis of water by acidic cations: the metal cations attract the water oxygen electrons releasing a proton. Thus, once the local pH reaches the hydrolysis pK_a of these different cations, hydronium is produced and is readily reduced at the electrode which gives rise to HER. However, it is also important to consider the density of these cations near the surface. In fact, for each valence group, the highest activity was found for the cation not only with high acidity but also weak hydration that helps cation accumulation at the OHP.

Decreased reorganization energy by cations. Huang *et al.* demonstrated the effects of cations on the reorganization energy associated with HER/HOR.[48] It was shown that the kinetics of HER/HOR on Pt can vary by two orders of magnitude depending on the cation type with faster kinetics associated with smaller cations (*e.g.*, Li^+), consistent with previous results. Through MD simulations, they demonstrate that structure-making (smaller) cations, such as Li^+, maintain their solvation shell, while structure-breaking (larger) cations, such as Cs^+, are partially desolvated. Those larger cations concentrate at the surface resulting in a higher dielectric constant at the interface, greater interfacial water reorganization energy, and a higher entropic barrier associated with the formation of adsorbed H from water. Thus, HER/HOR kinetics decrease with larger cations, especially at high pHs, due to the larger barrier for electron transfer in the Volmer or Heyrovsky steps involving water dissociation.

3.2. Oxygen evolution and reduction reactions

General trends. AMCs have been shown to influence OER and ORR as well. The size of the cation has been shown to change the activity of OER on various catalysts. In general, as the cation size increases, the OER activity increases. Cation effects for OER on Au electrodes showed higher activity for OER in the order of $K^+ > Na^+ > Li^+$ in alkaline conditions.[57] Raventos *et al.* studied Ni electrode systems with a focus on higher electrolyte concentrations for potential applications in industry.[58] They found that the activity trend is similar ($Rb^+ > Cs^+ > K^+ > Na^+ > Li^+$) to trends put forth for low concentration electrolytes in alkaline media. The authors suggest that smaller cations can intercalate in the Ni oxyhydroxide layered double hydroxides (NiOOH–LDH) and therefore stabilize the γ-NiOOH phase which results in a higher OER onset potential. It is important to mention that different preparation methods for alkaline electrolytes might lead to the presence of other

impurities which significantly impact the interpretation of cation effects. Therefore, researchers are encouraged to take strict precautions to eliminate unwanted artifacts, as discussed in the work of Márquez *et al.*[59]

Intermediate (de)stabilization for OER. AMCs have been observed to (de)stabilize OER reaction intermediates as a way to influence OER rates. Garcia *et al.* conducted studies on Ni-based electrodes in an attempt to decipher the intrinsic AMC effect on Fe-free Ni oxyhydroxide (NiOOH) catalysts.[22] They found a similar OER rate dependence on AMCs: $Cs^+ > Na^+ > K^+ > Li^+$. They show that the electrochemically active surface area (ECSA) is not influenced by the cation type. In fact, they propose that the cations interact with the superoxo intermediate ($NiOO^-$) which is better stabilized by larger cations, such as Cs^+, and therefore explaining the trend. Such a trend also held in the presence of Fe in the electrolyte.

AMCs have been shown to also affect OER rates for RuO_2 (110) electrodes in alkaline solutions.[23] The trend was similar where larger cations (*e.g.*, K^+) resulted in higher OER activity compared to smaller cations (*e.g.*, Li^+). Rao *et al.* explained that structure-breaking larger cations with less compact hydration shells lead to more isolated water molecules in the surroundings. This leads to a more reactive interfacial OH^- not stabilized by icelike water structures. Furthermore, the water molecules within the hydration shell of a larger cation are less acidic (*i.e.*, large pK_a) with reduced interactions for stabilizing adsorbed oxygen intermediates. These effects combined improve the kinetics of the rate-limiting step of $O_{ads} + OH^- \rightarrow OOH_{ads} + e^-$ (Fig. 4A). Thus, in this case, the improved OER activity by larger AMCs is caused by the destabilization of a key OER intermediate.

Influence on the interfacial water structure. As mentioned in our previous section, interfacial water plays a crucial role in electrochemical reactions. AMCs have demonstrated the ability to impact interfacial water structure by changing the ordering of water molecules close to the catalyst surface. Hou and co-workers' investigation revolved around the impact of different AMC electrolytes on the OER activity of surface-mounted

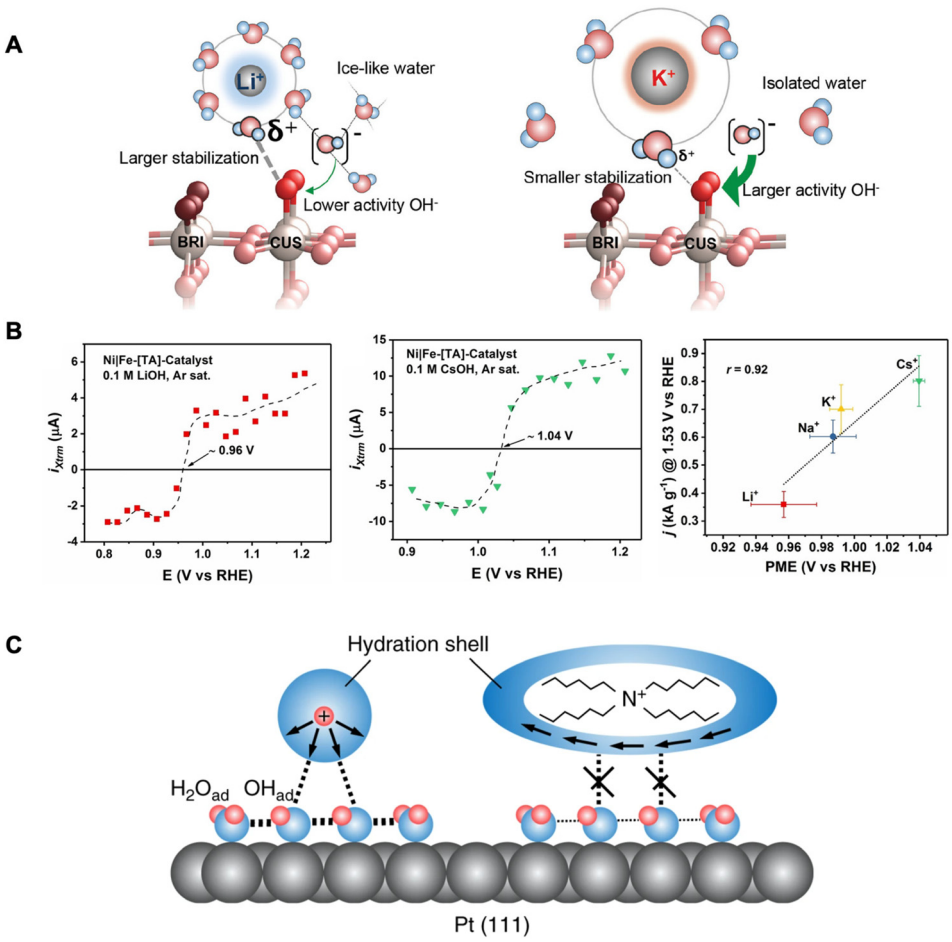

Fig. 4 (A) Schematic of the RuO_2(110) electrified interface in Li^+-containing electrolyte (left) and K^+-containing electrolyte (right). Reproduced from ref. 23 with permission from the American Chemical Society, copyright 2021. (B) LICT data demonstrating the current transients as a function of applied potential for different AMCs (left and middle) and electrocatalytic activity dependence on the PME in the presence of different AMCs. Reproduced from ref. 25 with permission from John Wiley and Sons, copyright 2022. (C) Schematic of the interfacial environment in the presence of hydrophilic and hydrophobic cations. Reproduced from ref. 60 with permission from Springer Nature, copyright 2018.

metal–organic framework (SURMOF) derived electrocatalysts based on NiFe(OOH).[25] It was found that the activity of the OER is influenced by the type of AMC following the expected trend: $Cs^+ > K^+ > Na^+ > Li^+$. The researchers conducted *in situ* Raman spectroscopy from which the results suggest that catalytic activity may be linked to the varying lengths of Ni–O bonds within the NiOOH active-phase structure. More importantly, the authors used the laser-induced current transient (LICT) technique to explore the AMC effects on the double-layer order/disorder. They found that the cation-dependence of OER activity is in line with the trend of the potential of maximum entropy (PME) at which the rearrangement of water molecules is facile leading to more favorable charge transfers during a reaction (Fig. 4B). The higher the PME, the looser the interfacial waters are during OER for more enhanced activity. Thus, the restructuring effects of large cations on interfacial water and therefore improving the kinetics of the OER were demonstrated.

Indirect pH effect. AMCs also vary the local pH environment. Görlin and coworkers studied $Ni_{65}Fe_{35}(OOH)$ electrocatalysts for OER where the different OER rates observed with different AMCs were attributed to indirect pH effects.[61] Specifically, they focus on the variance in AMC Lewis acidity and consequently the basicity of alkali hydroxides. The authors conducted X-ray absorption spectroelectrochemistry where larger cations were found to shift the Ni redox and OER process to lower potentials. They explain that with the use of larger cations, the electrolyte pH increases due to the higher basicity of the corresponding hydroxides (as was explained by their respective pK_b values). Furthermore, they observed an increase in activity with an increase in pH and larger cations exhibited a more substantial increase in activity. DFT calculations were used to show that cations do not significantly change the activities of Ni, Fe, or O lattice sites. These results suggest that the electrolyte pH may play a larger role in controlling OER activity.

Promoting the formation of catalytically more active phases. AMCs also promote the formation of catalytic active phases which in turn influence OER rates significantly. In a study conducted by Michael *et al.*, NiOOH thin films were used to study the OER activity in alkaline media with different AMCs.[62] The trend in activity remains more or less unchanged ($Cs^+ > K^+ \sim Na^+ \sim Li^+$). However, by tuning the Fe levels in the catalyst, the activity trend changed to $K^+ \sim Na^+ > Cs^+ > Li^+$. To further examine this phenomenon, the researchers conducted studies combining linear sweep voltammetry (LSV) and Raman spectroscopy to examine whether the variations in performance are associated with disparities in the structure of the active phase present. It revealed that, when Cs^+ is present, Raman peak positions for O–Ni–O bending and stretching modes are downshifted compared to when Li^+ is present. Similar shifts are observed with Fe present in the catalyst as well. The results suggested that Cs^+ induces a NiOOH active phase structure with longer Ni–O bonds that are more active for OER.

Intermediate (de)stabilization for ORR. Similar to OER, ORR is also affected by the presence of AMCs in the electrolyte. Specifically, it has been demonstrated that AMCs interact through non-covalent interactions with the reaction intermediates of ORR, such as OH_{ads}. Garlyyev *et al.* explored how different AMCs affect the ORR activities on high-index Pt surfaces, such as Pt(221) and Pt(331).[63] They conducted electrochemical measurements in both acidic and basic environments. Unlike Pt(111) whose activity increased, a decrease in activity was observed for both Pt(221) and Pt(331) when transitioning from an acidic to a basic environment. This was attributed to AMCs interacting with the surface sites of Pt. The ORR activity on stepped Pt electrodes exhibited a strong dependence on the identity of the AMC: $K^+ \gg Na^+ > Cs^+ > Rb^+ \approx Li^+$. They further demonstrate that the adsorption of OH species and oxide formation occur at a more positive potential in K^+-containing electrolytes compared to Li^+–containing electrolytes. Combining these effects of each AMC on the binding energies of OH ions and the hydration energy/shell size of solvated metal cations, they conclude that, beyond pH, AMCs significantly influence ORR activity on complex Pt surfaces.

With the same goal of elucidating how cations can affect ORR, Kumeda *et al.* studied the ORR activity on single-crystal Pt surfaces in acidic electrolytes, however with the presence of organic hydrophobic tetraalkylammonium (TAA) cations with varying alkyl chain lengths.[60] Their immediate observations were that the longer alkyl chain (n) TAA cations (*i.e.*, higher hydrophobicity), the higher the ORR activity following the trend: THA^+ ($n = 6$) $\gg$ TBA^+ ($n = 4$) > TEA^+ ($n = 2$) > TMA^+ ($n = 1$) $\approx$ $HClO_4$. Furthermore, *in situ* IR and X-ray CTR measurements demonstrate that in the presence of THA^+, less OH_{ads} coverage is found on Pt(111). They reason that hydrophobic cations such as THA^+ destabilize the OH_{ads} which is known to hinder ORR.[64] This occurs by THA^+ strengthening the hydrogen bonding in the primary hydration shell and restricting their coordination to species outside this shell (Fig. 4C). This weakens the interaction between the hydration shell around the THA^+ and OH_{ads} layer (with co-adsorbed H_2O) resulting in a more efficient interface for ORR.

3.3. Carbon dioxide and carbon monoxide reduction

General trends. Much like the other electrocatalytic reactions highlighted in previous sections, CO_2 and CO electroreduction are strongly influenced by the presence and identity of AMCs within the electrolyte. The general trend is that larger AMCs, such as Cs^+, tend to increase CO_2RR and CORR rates compared to that of smaller AMCs, such as Li^+.[65,66] The underlying mechanisms through which these AMCs exert their influence remain a subject of active investigation. So far, three ideas have been proposed: (1) AMCs can alter the local electric field to indirectly promote intermediate stabilization, (2) AMCs can directly interact with and stabilize reaction intermediates, (3) AMCs possess the ability to buffer the local pH and therefore control the concentration of reactants near the catalyst surface. It is therefore imperative to thoroughly understand how these AMCs may affect the reaction rates of CO_2RR and CORR to design efficient electrocatalytic systems with high activity and selectivity for value-added products.

Local electric field modulation for intermediate stabilization. AMCs have been shown to have significant effects on

the local electric field which in turn stabilizes reaction intermediates. Resasco *et al.* combined experimental and theoretical approaches to examine the effects of various AMCs on the intrinsic activity and selectivity of CO_2RR on different catalyst materials.[67] From potential sweep and steady-state potentiostatic measurements on Cu(100) and Cu(111) surfaces, they observed an increase in current density with cation size. In particular, the rates of formate, ethylene, and ethanol increased monotonically with increasing cation size (Fig. 5A). Experiments conducted on polycrystalline Ag and Sn showed a similar trend where the production of CO and formate increased with increasing cation size. DFT calculations utilized to interpret these results showed that the hydrated alkali metal cations, in general, at the OHP create an electric field that stabilizes the adsorption of surface intermediates having large dipole moments (Fig. 5A). This means a decrease in the adsorption energy of intermediates such as $*CO_2$ and *OCCO (* = site on the catalyst surface) which are key to CO_2 activation and formation of multicarbons, respectively. However, larger cations are more energetically favored to be found at the OHP than smaller cations (Fig. 5B). Therefore, a larger coverage of cations at the OHP is expected with increasing cation size leading to more of the intermediate stabilization effects and resulting higher activity.

Ringe *et al.* applied a multi-scale comprehensive model combining *ab initio* and continuum electrolyte models to understand the cation effects of CO_2RR.[69] Employing a modified Poisson Boltzmann method within the continuum framework, the authors observed significant alterations in the surface charge density and associated electric fields due to repulsive interactions among hydrated cations in the Helmholtz layer. Specifically, they found that weakly hydrated cations (*e.g.*, Cs^+) with smaller *hydrated cation radii* exhibit weaker repulsion and accumulate at the OHP at a higher concentration. This induces a higher surface charge density and a stronger electric field, leading to enhanced CO_2RR. Their model closely matched the experimental trends seen for Ag and Cu electrodes in CO_2RR.

In another work, Gu *et al.* elucidated the cation effects on CO_2RR in highly acidic environments (pH = 1.0) with SnO_2/C, Au/C, and Cu/C nanoparticle catalysts.[68] The authors demonstrate that hydrated alkali cations hinder hydronium ion

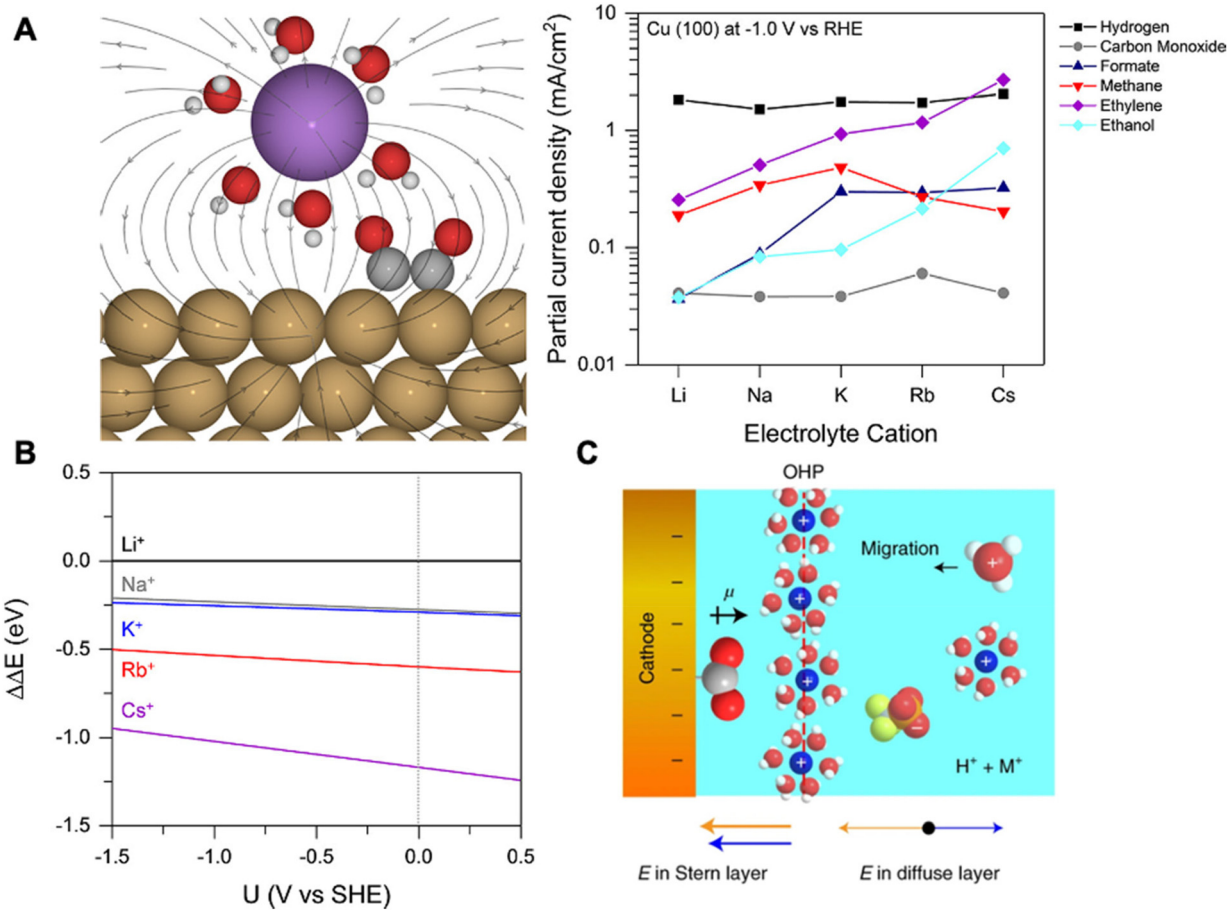

Fig. 5 (A) Schematic of hydrated cation electrostatic interactions with intermediates having large dipole moments (left), the effect of cation size on various product formations (right). (B) The energy required to bring different solvated cations from the bulk to the OHP at the Cu(111) facet. Reproduced from ref. 67 with permission from the American Chemical Society, copyright 2017. (C) Schematic of the electrode–electrolyte interface showing the accumulation of hydrated K^+ at the OHP. Reproduced from ref. 68 with permission from Springer Nature, copyright 2022.

migration decreasing HER while simultaneously promoting CO_2RR through reaction intermediate stabilization. In the presence of K^+ in acidic electrolytes, HER was surprisingly well suppressed with formic acid (max FE 88%) and CO (max FE 91%) as major products for SnO_2/C, and Au/C, respectively. For Cu/C, a plethora of products were detected, including formic acid, CO, methane, ethylene, and ethanol, with ethylene FE as high as 25%. Simulations based on the Poisson–Nernst–Planck (PNP) model showed that hydrated K^+ and hydronium ions compete for adsorption creating a chemically inert hydrated K^+ layer formed at the OHP (Fig. 5C). This layer shields the electric field from the cathode, therefore suppressing hydronium ion migration and HER. Moreover, the key intermediates for CO_2RR (*e.g.*, $*CO_2$, *OCCO) are stabilized by dipole-field interactions between the intermediate dipole (pointing away from the catalyst surface) and electric field created by cations within the Stern layer (pointing towards the catalyst surface) enhancing CO_2RR (Fig. 5C). Furthermore, the authors reached a similar conclusion where the increase in intrinsic cation size (*e.g.*, Cs^+) results in a higher concentration of cations at the OHP and the stronger stabilization of those intermediates.

Direct local interactions for intermediate stabilization. Some researchers have proposed direct AMC interaction with intermediates leading to intermediate stabilization and therefore enhancement of CO_2RR. Monteiro *et al.* coupled CV and scanning electrochemical microscopy (SECM) experiments with DFT to study the effects of AMCs on the CO_2RR activity of different catalysts such as Au, Ag, and Cu.[65] The main observation was that, in the absence of cations, the CO_2RR did not take place in mildly acidic solutions (pH = 3) (Fig. 6A). Furthermore, CO production increased following the trend: $Cs^+ > K^+ > Na^+ > Li^+$. AIMD calculations showed a strong correlation between activity and the cation size where the ones with a softer hydration shell (*e.g.*, Cs^+) are better able to bind to the oxygen atom of CO_2 adsorbed helping its stabilization. The authors highlight the importance of having partially desolvated cations where they allow not only the medium-range electric dipole and electric field interaction (as described in the previous section) but also the short-range electrostatic interaction between the metal and oxygen of the CO_2 (Fig. 6B). Thus, they conclude that the cation dependence is due to both their different concentrations at the OHP as well as their different capability of specifically interacting with negatively charged adsorbates.

Qin *et al.* reached a similar conclusion demonstrating cation-coordinated inner-sphere CO_2 reduction by studying the effects of AMCs on CO_2RR on Au surfaces using atomic-level

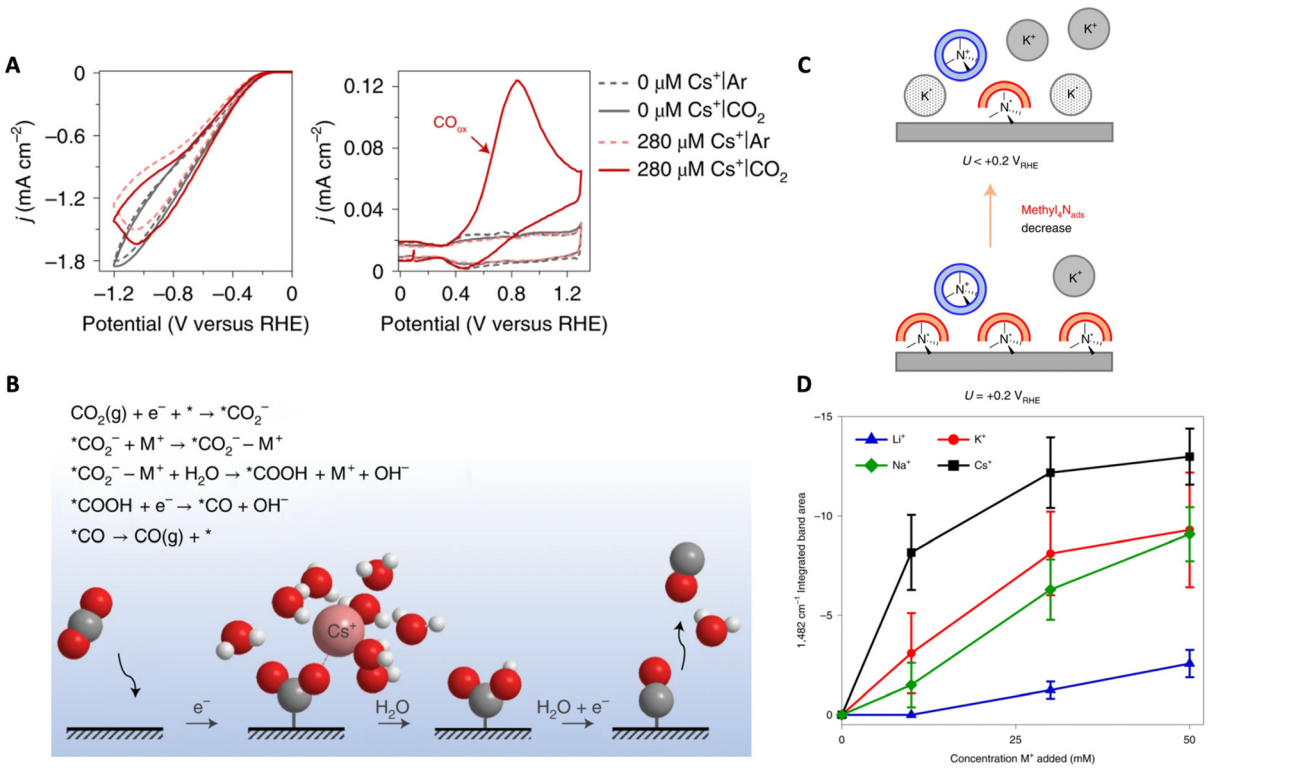

Fig. 6 (A) Cathodic and anodic scans recorded in argon and CO_2 atmospheres with different concentrations of Cs^+. (B) Schematic demonstrating the interaction of the cation with the reaction intermediate ($*CO_2^-$) as well as a reaction mechanism for the CO_2RR. Reproduced from ref. 65 with permission from Springer Nature, copyright 2021. (C) Schematic demonstrating the replacement of $methyl_4N_{ads}$ by specifically adsorbed K^+. (D) Coverage of specifically adsorbed AMCs at −0.45 V *vs.* RHE measured by integrating the area of the 1482 cm^{-1} band as a function of bulk AMC concentration. Reproduced from ref. 66 with permission from Springer Nature, copyright 2022.

simulations.[70] Through slow-growth (SG) AIMD methods, the authors generated a comprehensive free energy diagram for the CO_2RR for the first time. It was observed that, in the presence of K^+ at the Au–water interface, CO_2 reduction is favorable with the CO_2 activation step only exhibiting a 0.66 eV barrier by cation coordination. Simultaneously, the competing HER is significantly suppressed, displaying a 1.27 eV barrier in the rate-limiting Volmer step ($H_2O + e^- + * \rightarrow *H + OH^-$). Furthermore, the simulations confirmed that $*CO_{atop}$ (linearly bonded CO) is the active intermediate in CO_2 electroreduction while $*CO_{bridge}$ (bridge bonded CO) is a kinetically inert spectator.

Partial dehydration and specific adsorption of AMCs at the interface have been described in other works as well. Ovalle *et al.* studied the effect of AMCs on the CO_2 reduction to CO on polycrystalline Au by using tetramethylammonium ($methyl_4N^+$) as a vibrational probe.[66] Using ATR-SEIRAS and probing the asymmetric deformation band of CH_3 of $methyl_4N^+$ at the Au–electrolyte interface, the authors showed that, with an increase in K^+ concentration, a negative band attributed to the non-hydrated specifically adsorbed $methyl_4N^+$ (1482 cm^{-1}) grows due to their displacement by K^+ (Fig. 6C). Using this band as a spectroscopic measure for the coverage of specifically adsorbed cations, the $Li^+ < Na^+ < K^+ < Cs^+$ trend was found (Fig. 6D). Furthermore, they were able to associate the degree to which these cations displace $methyl_4N_{ads}$ (*i.e.* degree of cation coverage) with their free energies of hydration. This observation demonstrates that metals with a soft hydration shell have a higher tendency to specifically adsorb on the electrode surface. Further, the partial current density for CO was shown to increase with increasing cation coverage. Thus, the authors suggest that direct cation–intermediate interactions may be possible with these specifically adsorbed cations.

Shin *et al.* employed density functional theory in a classical explicit solvent (DFT-CES) to study the interactions of AMCs with key intermediates of CO_2RR.[71] From these calculations they identified 6 crucial intermediates ($*CO_2$, *COOH, *CHO, *OCCO, *OCCOH, and *HOCCOH) that can be coordinated to a cation during the production of C_1 and C_2 products such as CO, CH_4, and C_2H_4. They also performed electrochemical measurements which revealed that the activity trend for CO and C_2H_4 formation on electrodes like Ag and Cu follows the order: $Cs^+ > Rb^+ > K^+ > Na^+ > Li^+$, while for CH_4 formation the trend is the opposite. These results coupled with results by Chan and coworkers demonstrating the dependence of CO_2RR products on pH,[72] the authors suggest that the rate-determining step (RDS) for CO and C_2H_4 formation involves a cation-coupled electron transfer (CCET), while the RDS for CH_4 formation involves a proton-coupled electron transfer (PCET). The variation in cation-dependent activity is attributed to the differing stabilization capabilities of various AMCs as mentioned in previous studies. Furthermore, the authors demonstrate first-order kinetics on the surface charge density for CO and C_2H_4 formation which is in line with what is expected assuming the cation-coupled electron transfer RDS.

As part of this effort, Kim *et al.* demonstrated a novel approach, so-called the nanoparticle/ordered-ligand interlayer (NOLI), which almost exclusively reduces CO_2 to CO due to the cation effect.[73] NOLI contains Ag nanoparticles which have tetradecylphosphonic acid (TDPA) ligands "floating" in the vicinity under negative bias. At the interlayer between the Ag NP surface and ligand, CO_2RR to CO occurs with approximately 97% CO selectivity as well as 2 orders of magnitude increase in intrinsic activity when compared to polycrystalline Ag foil. Utilizing X-ray absorption near edge structure (XANES) and AIMD simulations, the authors showed the presence of dehydrated cations (*e.g.*, K^+) within the interlayer where the phosphonate group (from TDPA ligands) anchors the dehydrated cation. Through the first-principles free energy calculations, this structure was found to facilitate the activation of CO_2 by the dehydrated cation. Furthermore, even with strongly solvated cations such as Li^+ which is normally not favored for CO_2RR, having the NOLI structure allowed achieving a 70% CO selectivity (in contrast with the Ag foil only at 3%). Similar improvements were demonstrated with other metals, such as Au and Pd. While it is evident that AMCs affect the rates and selectivity of CO_2RR, their impacts could be strengthened by partially removing their hydration shells and allowing direct interaction with intermediates.

Cation effect through local pH buffering. Some works have focused on the pH buffering capability of AMCs which affects CO_2RR. One of the earlier works was by Singh *et al.* studying the effects of AMCs on the CO_2RR by Ag and Cu.[74] They also observed an increase in current density and higher selectivity for CO_2-reduced products with increasing AMC size. The authors used a multiphysics electrochemical model to show that larger cations can act as better pH buffers near the electrode surface which tend to turn basic under operating conditions (due to hydroxide formation). It was shown that, with Cs^+, the surface pH is 7, whereas with Li^+, it is 9. It was explained that larger cations have significantly lower pK_a values near a charged surface and this leads to better pH buffering locally. As a result, there is a greater local CO_2 concentration with larger cations (*i.e.*, low surface pHs) that increase the activity and selectivity for CO_2RR.

Building upon this previous study, Ayemoba *et al.* experimentally studied the buffering effect by probing the pH at the Au–electrolyte interface using ATR-SEIRAS.[75] They managed to probe the pH through the inversely proportional relationship between H^+ concentration and the ratio of $CO_2 : HCO_3^-$ peak integrated intensity. The authors observe an increase in pH during CO_2RR regardless of the AMC. However, with larger AMCs, the pH increased minimally supporting the earlier work by Singh *et al.*[74]

Zhang *et al.* used a rotating ring-disc electrode (RRDE) with an Au disk and Pt ring to detect local pH changes during the CO_2RR.[76] They observed a −86 mV pH^{-1} shift in the CO (which is a product of the Au disk) oxidation peak by the Pt-ring which they used to directly probe the pH changes near the electrode surface. Utilizing this technique, they found that local basicity decreased with the cation identity following the

trend: $Li^+ > Na^+ > K^+ > Cs^+$ in agreement with previous studies.[74,75] They also concluded that larger cations having larger buffering capability result in a lower local pH and therefore enhance CO_2RR.

Even though cationic pH buffering arguments might seem reasonable, latest studies suggest that it might not be the case. For example, Monteiro *et al.* argue that AMC pH buffering does not play a major role in the enhancement of the CO_2RR.[65] They suggest that, if local pH effects are key, the CO_2RR should still take place, even in the absence of cations, in a pH = 3 solution. However, they find that the absence of AMCs in fact eliminates the CO_2RR from taking place at all, which contradicts the pH buffering theory and supports other theories for the cation effects.

Multivalent cation effect on CO_2RR. As an extension to the effect of AMCs on CO_2RR, Wang *et al.* utilized *in situ* electrochemical scanning tunneling microscopy (ECSTM) to study the effects of multivalent cations such as Mg^{2+} on the CO_2RR on a cobalt phthalocyanine (CoPc) catalyst.[77] The authors observed that, in an Mg^{2+}-containing electrolyte, there is a higher reductive current for CO_2 than in an electrolyte without Mg^{2+} indicating Mg^{2+} facilitates CO_2RR (Fig. 7A). From *in situ* ECSTM experiments, it was found that high contrast species are CO_2 adsorbed on CoPc. Furthermore, the contrast in a Mg^{2+}-containing electrolyte is higher than in the Mg^{2+}-free electrolyte indicating the formation of the CoPc–CO_2–Mg^{2+} complex. They studied the addition of different concentrations of Mg^{2+} and observed that CO_2 coverage increased with increasing cation concentrations until a plateau of approximately 30.8% when [Mg^{2+}] exceeded 30 mM (Fig. 7B). Moreover, potential step experiments to elucidate the CO_2 adsorption dynamics showed that the rate constant for CO_2 adsorption is higher in the presence of Mg^{2+} showcasing the cation's influence on the activation energy of adsorption. The rate constant for desorption was found to be lower in the presence of Mg^{2+} suggesting that the cation stabilizes CO_2 adsorbed. Further DFT calculations corroborated these results where a larger ΔG was obtained for the formation of the CoPc–CO_2–Mg^{2+} complex to that of the CoPc–CO_2.

Monteiro *et al.* studied the effects of various cations, that are AMCs and multivalent cations, on the CO_2RR in a mildly acidic (bulk pH 3) condition.[24] The authors found that strongly acidic cations (*e.g.*, Ce^{3+}, Nd^{3+}) only favor CO_2RR at low overpotentials till they start to undergo hydrolysis (*i.e.*, at high overpotentials where the local pH shifts basic) favoring HER. At high overpotentials, a higher CO activity was observed for electro-

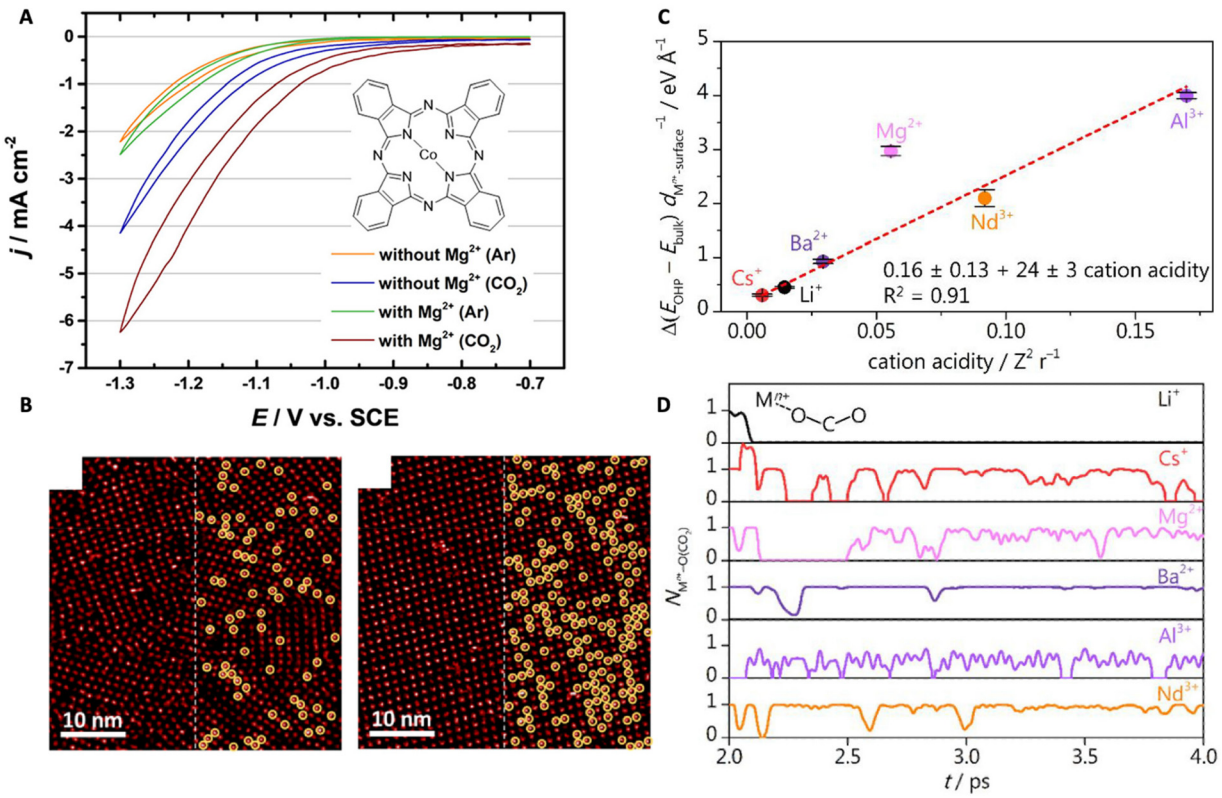

Fig. 7 (A) Cyclic voltammograms of the CoPc-modified Au(111) electrode showing the effects of Mg^{2+} on CO_2RR (the inset shows the chemical structure of the CoPc molecule). (B) STM images of the self-assembled monolayer of CoPc on the gold surface in the CO_2 environment at different concentrations of Mg^{2+}: 0.005 M Mg^{2+} (left), 0.03 M Mg^{2+} (right). Reproduced from ref. 77 with permission from the American Chemical Society, copyright 2022. (C) The relationship between the thermodynamic driving force for cation accumulation and cation acidity. (D) AIMD simulation demonstrating the coordination between the cation and CO_2. Reproduced from ref. 24 with permission from the American Chemical Society, copyright 2022.

lytes containing less acidic cations, such as Cs^+, Li^+, Ba^{2+}, and Ca^{2+}. A quantitative comparison among them led to a CO activity trend that is $Ca^{2+} < Li^+ < Ba^{2+} < Cs^+$. This complex behavior is due to the various factors that are involved in cation effects. AIMD simulations show that softly hydrated cations accumulate at the OHP at a higher concentration, and the lower the acidity, the larger their accumulation for intermediate stabilization (Fig. 7C). This is the reason why Cs^+ and Ba^{2+} are better for CO_2RR. However, for the short-range coordinative interaction between the cation and $*CO_2^-$ that facilitates CO_2 activation, trivalent cations (*e.g.*, Nd^{3+}) are more effective intrinsically (Fig. 7D). However, they also promote water dissociation at basic pHs leading to faster kinetics for HER at high overpotentials and thus, were only effective for CO_2RR at low overpotentials.

Cation effect on the carbon monoxide reduction reaction (CORR). In addition to the cation effects on CO_2RR, AMCs have been shown to affect the activity of CORR. The previously discussed work of Resasco *et al.* found that the positive influence of cations were both applicable to CO_2RR and CORR.[67] It was demonstrated that the impacts of cation size on the CORR mirror the effects observed during CO_2RR on Cu(100) catalysts. This observation supports that cations play a broader role in stabilizing reaction intermediates and transition states, rather than merely affecting the initial activation step of the CO_2RR.

Pérez-Gallent and coworkers explored the effects of AMCs on the CORR on Cu single crystals where they showed that the surface structure of Cu as well as the applied potential influence the cation effects.[78] From online electrochemical mass spectrometry (OLEMS) and high-performance liquid chromatography (HPLC), they showed that cation effects are potential-dependent. Larger cations (*e.g.*, Cs^+) increase the selectivity towards ethylene production at low overpotentials while methane is favored at more negative potentials, a trend found in all Cu structures. The authors also showed that the cation effects are structure sensitive with the onset potential for ethylene formation most positive on Cu(100). The RDS for CO to methane or ethylene formation on Cu(100) is CO hydrogenation, and this process is significantly more efficient when alkaline cations are present for a CO dimer (to *OCCOH) as opposed to a CO monomer (to *CHO) based on DFT. Furthermore, FTIR studies showed the presence of a hydrogenated dimer intermediate (*OCCOH) at low overpotentials. The formation of this intermediate depends on cation size as it is detected in the presence of Li^+, Na^+, and K^+, but not in the presence of Rb^+ and Cs^+. DFT calculations explained the FTIR observations suggesting that the potential necessary to form *OCCOH from *CO in the presence of Cs^+ is more negative compared to smaller cations such as Li^+. Moreover, the activation energy required for any intermediate formation (*CO, 2*CO, *OCCO, *CHO, and *OCCOH) is decreased in the presence of cations highlighting the intermediate stabilization effects of AMCs. Overall, these results demonstrate the clear effect of AMCs on the CORR with larger cations tending to promote the pathways with intermediates more effectively than smaller cations.

Similarly, Malkani *et al.* studied the effects of AMCs on the CORR on polycrystalline Cu in alkaline media.[79] The authors demonstrated that larger AMCs (not considering the hydration shell size) promote CO reduction on Cu(poly) in alkaline media. They observed a trend where the rates of both CORR and HER increase with cation size. Moreover, the FE for CORR products increased with increasing AMC size. *In situ* SEIRAS investigations showed that the CO adsorption distribution varies with different cations: the ratio of CO adsorbed on step sites to CO adsorbed on terraces increased from Li^+ to K^+ then leveled off. This indicates the existence of an interaction between AMCs and the CO adsorbed. They also measured Stark tuning rates (indicative of EDL electric field strength) which exhibited the following trend: $Cs^+{\cdot}xH_2O \sim Rb^+{\cdot}xH_2O \sim K^+{\cdot}xH_2O > Na^+{\cdot}xH_2O > Li^+{\cdot}xH_2O$. This suggests that the thickness of the double layer is thinner for cations like K^+ compared to Li^+. Thus, the interfacial electric field seems mostly responsible for the enhanced CORR activity from Li^+ to K^+. However, such an effect plateaus beyond K^+ while the CORR continuously improves suggesting a non-electric field (NEF) component within the cation effect on CORR. Further investigations with cations such as the K^+ chelated crown ethers were conducted to show how the electric and NEF components of the cation effect could be affected by the chemical structure and charge distribution of cations.

4. Anion effects on electrocatalytic reactions

4.1. Water electrochemistry (HER/HOR/OER/ORR)

General trends. In addition to cations and water molecules, anions have been observed to influence the electrocatalytic reactions discussed thus far. Typically, for water electrochemistry, the anionic effects are primarily observed during ORR, such as the competition for surface sites between anions and reaction intermediates.[80] The absence of significant anionic effects in HER is attributed to the high adsorption affinity of protons (in H-UPD and HER potential regions) hindering anion adsorption and any form of competition between the two species.[81,82] Moreover, on Pt catalysts, the ORR activity was influenced depending on the anion present in the electrolyte following the general trend: $HClO_4 > H_2SO_4 > H_3PO_4 > HCl$ depending on the adsorption energies of each anion.[82,83]

It is also of great importance to understand how anions affect the ORR activity as future technologies such as proton exchange membrane fuel cells (PEMFCs) utilize Nafion membranes which are comprised of sulfonate groups. Nafion membranes are essential in these systems as they provide a proton conductive path as well as act as a binder in the catalyst layer.[84] Therefore, understanding how anions influence ORR is essential to be able to design efficient devices, such as fuel cells and metal–air batteries, for future sustainability applications.

Anionic effects on the oxygen reduction reaction through surface site blocking. Anionic effects on the ORR are an area

of active investigation. You *et al.* studied the effects of impurity anions on the activity of a Pt/C.[85] The authors found that anions such as CO_3^{2-}, F^-, Cl^-, Br^-, and SO_4^{2-} had minimal effects on ORR activity as evidenced by the minimal change in the half-wave potential. However, anions such as SO_3^{2-}, I^-, and S^{2-} were found to have significant poisoning effects. The authors proposed that, under ORR potentials, it is easier to adsorb anions such as S^{2-} than anions such as F^-, therefore inducing catalyst poisoning and hindering ORR.

Jusys and Behm conducted an in-depth study on the effects of anions on the ORR on annealed gold films in different electrolytes such as sulfuric and perchloric acids as well as sodium hydroxide.[86] The authors observed ORR activity inhibition due to the adsorption of the anionic species onto the surface of the electrode and limiting the number of active sites. In general, ORR activity followed the trend: NaOH > $HClO_4$ > H_2SO_4 as evidenced by a more positive onset potential in alkaline media as well as in perchloric acid solutions compared to sulfuric acid electrolytes. Further results from potentiodynamic studies revealed that in acidic media the ORR proceeds towards the formation of superoxides while in alkaline media the reaction favors the $4e^-$ pathway at high overpotentials. The enhanced activity and selectivity observed in the $4e^-$ pathway under alkaline electrolyte conditions is due to a densely packed OH_{ads} layer. This adlayer may serve as a scaffold for the ORR, potentially through an outer-sphere ORR process. In contrast, at lower potentials and, thus, diminished OH_{ads} coverages, the reaction seems to progress through the interaction between $O_{2,ads}$ and the Au site.

In another study, Zeledón *et al.* combined electrochemical and physical characterization, revealing the different effects of acidic electrolyte anions on ORR activity and selectivity on Ag and Pd catalyst thin films.[83] Through CV and Tafel slope analysis, they revealed that on Ag (weak oxygen binding) the ORR activity trend follows: $HClO_4$ > HNO_3 > H_2SO_4 > H_3PO_4 > HCl ≫ HBr, and on Pd (strong oxygen binding) the trend follows: $HClO_4$ > H_2SO_4 > HNO_3 > H_3PO_4 > HCl ≫ HBr (Fig. 8A). The authors claim that the observed trends are related to competitive anion adsorption as well as non-covalent interactions. To understand these effects, the authors conducted DFT calculations of the adsorption free energy of each anion. From these calculations they found that Cl^- and Br^- were chemisorbed to the surface while the anions NO_3^-, HSO_4^-, SO_4^{2-}, $H_2PO_4^-$, and HPO_4^{2-} may physisorb onto the surface (Fig. 8B). Their results

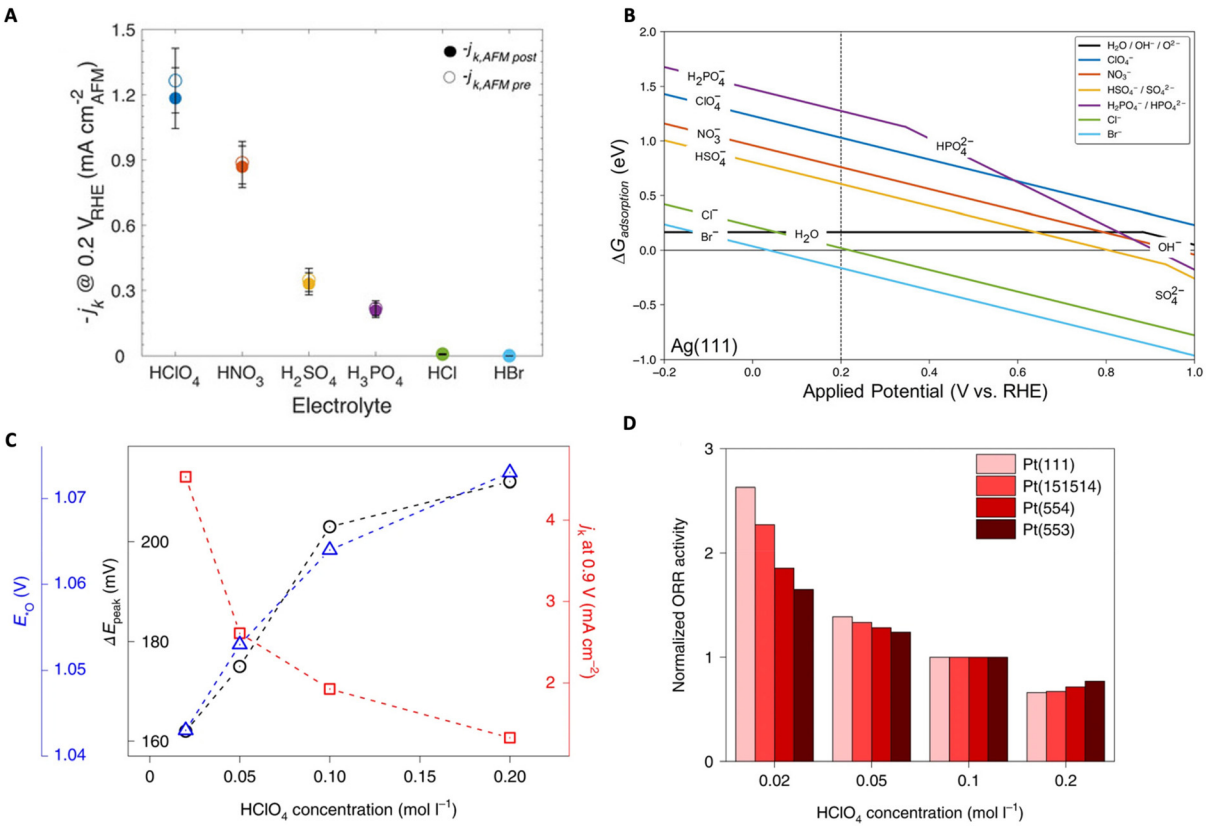

Fig. 8 (A) Average ORR specific activity normalized by exposed surface area before (empty circles) and after (filled circles) AFM measurement for Ag. (B) Adsorption free energy of anions as a function of applied potential (*vs.* RHE) on an Ag(111) surface. Reproduced from ref. 83 with permission from John Wiley and Sons, copyright 2021. (C) Plot showing the peak-to-peak potential difference between the anodic and cathodic peak of the *O ↔ *OH transition (black), the specific activities (red), and peak potentials of *O from CV (blue) as a function of $HClO_4$ concentration. (D) Normalized ORR activities on different Pt surfaces as a function of $HClO_4$ concentration. Reproduced from ref. 87 with permission from Springer Nature, copyright 2022.

indicate that, in the presence of the two halides (Cl^- and Br^-), surface active sites are blocked and therefore decrease the total number of active sites available for molecular oxygen to interact with the surface, thus hindering the ORR.

Kamat *et al.* further studied the effect of various acid anions on the ORR/OER on Pt(poly) catalyst.[82] The ORR activity trend was observed to follow $HClO_4$ > HNO_3 > H_2SO_4, with each acid's onset potential becoming less positive. Similarly, the OER activity trend was noted as $HClO_4$ > HNO_3 ~ H_2SO_4. To further understand these trends, the adsorption free energies of the anions were calculated using DFT where it was shown that the adsorption energies followed the trend: ClO_4^- > NO_3^- ~ SO_4^{2-} demonstrating that certain anions strongly adsorb to the catalyst surface and hinder ORR through active site blocking. Furthermore, in $HClO_4$, there is less anion adsorption leading to the increase in OER rates as well due to higher availability of active sites. These results demonstrate that the anionic effects are predominantly due to competitive adsorption rather than non-adsorbed anion–intermediate interactions.

Working with non-precious-metal catalysts, specifically a Fe/N/C catalyst, Holst-Olesen and coworkers studied the anionic effects on the ORR in various acidic electrolytes.[26] They found that the anions had less poisoning effects on the Fe/N/C compared to the Pt. On Pt(poly), ORR activity decreased in the order $HClO_4$ > H_2SO_4 > H_3PO_4 > HCl as previously mentioned, while for the Fe/N/C catalyst, the activity followed the trend H_3PO_4 > $HClO_4$ ~ H_2SO_4 > HCl. Using DFT calculations, it was shown that for both Pt(111) and Fe/N/C catalysts, phosphoric acid interacts strongly with the catalyst compared to the expected ORR intermediates and, therefore likely to decrease ORR activity. However, the observed enhancement of ORR on Fe/N/C in the presence of phosphoric acid can be attributed to the 2D structure of Fe/N/C where, despite anion adsorption, the opposite side can function as the ORR active site. Further DFT calculations demonstrated that the stronger binding acid (H_3PO_4) altered the FeN_4 site and decreased the thermodynamic barrier for the RDS for ORR.

Luo and Koper focused on the effect of non-specifically adsorbed (NSA) anions (*e.g.*, methanesulfonic acid (MSA), perfluorosulfonic acid (PFSA) ionomers) on the ORR activity of single crystal Pt electrodes and found a general inhibitory effect.[87] They utilized the electrochemical transition between *O ↔ *OH, where both are key ORR intermediates, as a kinetic descriptor to shed light on the effect of NSA anions on the ORR rates. It was observed that, with higher concentration of NSA anions, the ORR activity on Pt (111) declined as well as the rate of *O ↔ *OH transition measured by the peak-to-peak separation (ΔE_{peak}) in CV (Fig. 8C). Further studies utilizing Nafion-covered Pt(111) catalysts demonstrated that Nafion also suppresses ORR together with the declined reversibility of the *O ↔ *OH transition. Furthermore, they conducted similar studies on stepped Pt surfaces where not only the kinetic descriptor predictions were verified (*i.e.*, ORR activity decreased with $HClO_4$ concentration) but also Pt (111) was shown to exhibit the highest sensitivity to the anion inhibitory effects (*i.e.*, (111) terraces are most sensitive) (Fig. 8D). The authors also demonstrate that this kinetic descriptor applies well to cases where cations are present. It is speculated that a strong interaction between the anions (or cations) and the *OH layer exists causing slowed kinetics for the *O ↔ *OH transition, but as stated by the authors, further in-depth investigations are necessary.

4.2. Carbon dioxide reduction

General trends. Besides cations, anions have been shown to affect the kinetics of the CO_2RR. Specifically, halide anions are known to increase CO_2RR rates with increasing halide anion size following the trend F^- < Cl^- < I^- regardless of the electrode material.[88–90] The mechanism is still under active investigation. Some claim that halides induce morphological changes to the catalyst surface thereby influencing the reaction, while others argue that halide anions facilitate CO_2RR through intermediate stabilization or local electric field modulation.[88,91,92] Here, we focus on the research indicating that halide anions within the interfacial liquid influence the CO_2RR, rather than the reports that show the indirect effect of halides *via* surface structure changes of catalysts. Besides halides, other anions, such as HCO_3^- and HPO_4^{2-}, have also been shown to influence the CO_2RR through dynamic equilibrium effects with CO_2 and local pH changes.

Effects of halides on the carbon dioxide reduction reaction. Halides, like AMCs, have been shown to influence the electrocatalytic reduction of CO_2. Varela *et al.* investigated the anionic effects on Cu catalysts by keeping the concentration of the $KHCO_3$ buffer constant (0.1 M) and varying the halide identity through the addition of various concentrations of KA (where A = halide).[88] It was shown that CO selectivity increased for Br^- and Cl^-, mainly due to the drop in the H_2 formation rate, while CO formation rate minorly improved or diminished. In I^--containing electrolytes, the formation of other hydrocarbons through CO protonation (which is considered the RDS), particularly methane, was enhanced, while H_2 and CO rates were maintained similar. Utilizing DFT calculations conducted by McCrum and coworkers,[93] the authors conclude that I^- can adsorb more strongly and the charge retention increases in the order of I^- < Br^- < Cl^-. Thus, I^- is capable of donating more of its negative charge to the catalyst surface. This increases the negative charge on the surface of the Cu catalyst enhancing the interaction with the partially positively charged C atom of the CO_2 (or CO) molecule and favoring its protonation leading to methane.

In another work, Huang *et al.* studied the effects of halide anions on the CO_2RR on single crystal Cu catalysts such as Cu (100) and Cu(111) in unbuffered 0.1 M $KClO_4$ as well as KA (where A = halide) electrolytes.[94] The authors focused on how the halides affect CO_2RR selectivity, specifically for the C_{2+} products. The FE of C_{2+} products increased following a similar aforementioned anionic trend: ClO_4^- < Cl^- < Br^- < I^- (Fig. 9A) and this was due to the partial current densities increasing for ethylene and ethanol. In the unbuffered KI electrolyte, the FEs for ethylene and ethanol were the highest at 50% and 16%,

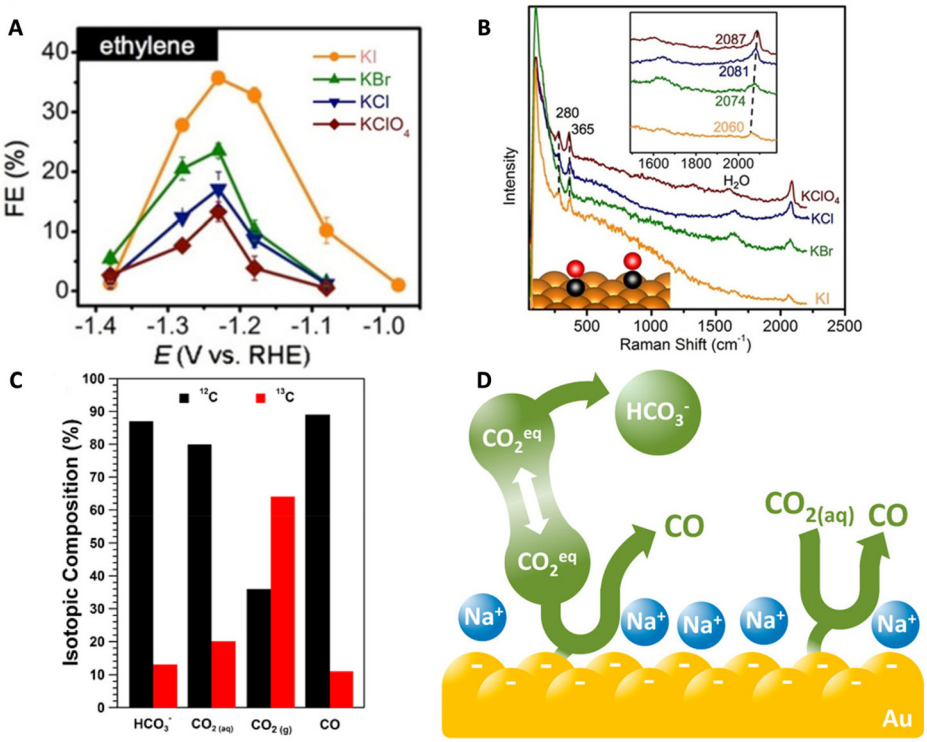

Fig. 9 (A) FE for ethylene produced on a Cu(111) catalyst in 0.1 M $HClO_4$, KCl, KBr, and KI electrolytes. (B) *In situ* Raman spectra of a Cu(pc) catalyst during CO_2RR in the same electrolytes. Top inset shows the red shift of the CO stretching band and the bottom inset is a schematic of the CO adsorbed onto the Cu(pc) surface. Reproduced from ref. 94 with permission from John Wiley and Sons, copyright 2018. (C) Isotopic compositions of HCO_3^-, $CO_{2(aq)}$, $CO_{2(g)}$, and CO produced during the CO_2RR. (D) Schematic demonstrating that the main source of CO_2 is the HCO_3^- through which there is a rapid equilibrium with CO_2 within the electrolyte. Reproduced from ref. 12 with permission from the American Chemical Society, copyright 2017.

respectively, with the overall FE for C_2 and C_3 products reaching 74%. The authors also found that in the presence of I^-, more CO_{ads} led to increasing C_{2+} production. *In situ* Raman spectroscopy showed a red shift in the C–O stretching mode from 2087 cm^{-1} to 2060 cm^{-1} when varying the electrolyte from $KClO_4$ to KI demonstrating the effect of anions on the environment of CO (Fig. 9B). The reason for the enhancement in C_{2+} formation was explained as a combined effect of a higher *CO population and the modified electronic structure of local Cu sites due to the adsorbed I^-.

Studying the effects of halide anions on the CO_2RR has been a challenge since halides have been shown to affect the morphology of the catalyst surface during CO_2 reduction.[88,94] The convolution of morphological changes and halide anion presence renders it difficult to determine the origin of CO_2RR activity enhancement. To deconvolute these variables, Yuan *et al.* pretreated CuO-nanosheets (Cu–ONS) electrodes in order to reach a morphologically stable surface state prior to CO_2 reduction investigations.[90] In addition, they added a supporting K_2SO_4 electrolyte to minimize any further morphological changes that may occur during the CO_2 reduction. It was found that the FE of C_2 products, specifically ethylene and ethanol, increases with increasing halide concentration with a maximum FE of C_{2+} products ~84.5% in I^--containing media. This was due to the partial current densities increasing for ethylene, ethanol, and propanol with increasing I^- concentration. The authors utilized *in situ* ATR-SEIRAS and found that, in a halide-containing electrolyte, the CO_{ads} band red-shifted to lower wavenumbers with increasing halide concentration. Similar to the earlier works, they explain that when halides specifically adsorb onto the surface, negative charges from the anions transfer to the CO_{ads} which enhances CO adsorption strength and C–C coupling.

Zhang *et al.* studied the effects of halides on nanoporous Ag catalysts.[89] In the presence of F^-, Cl^-, and Br^-, the CO FE is enhanced with the maximum FE found in the presence of Br^-. This was due to an enhancement in CO partial current density while that of H_2 showed the opposite trend. Interestingly, in the presence of I^-, the Ag catalyst demonstrated the poorest catalytic activity until −0.69 V *vs.* RHE. However, at potentials more negative than −0.89 V *vs.* RHE, the CO FE and partial current density was the highest surpassing the effects of Br^- and reaching a maximum FE of 90.3%. To further explore how halides affect the CO_2RR, the authors studied the Tafel kinetics. In theory, the RDS for the CO_2 to CO reaction is a single electron transfer step resulting in $*CO_2^-$ with a Tafel slope of 118 mV dec^{-1}. All Tafel slopes calculated for the systems containing halides were smaller than this theoretical value indi-

cating a change in the RDS from a single electron transfer step to the proton transfer chemical step. Moreover, the Tafel slopes decreased with increasing anion size indicating accelerated kinetics of the CO_2RR. With DFT calculations, they found that the binding affinity of the key intermediate COOH increased with increasing halide size with a maximum value of −191.45 meV in the presence of I^-. This suggests that halide anions, especially I^-, promote increased adsorption of COOH thereby decreasing the required overpotential for the CO_2RR.

Influence of supporting electrolyte anions on the CO_2RR. Other than halide anions, other anions that are usually used as supporting electrolyte anions, such as HPO_4^{2-}, SO_4^{2-}, and HCO_3^-, have also been shown to influence the CO_2RR.[12,95] Dunwell *et al.* investigated the molecular realm of the electrode–electrolyte interface to understand the role of bicarbonate anions on the CO_2RR of Au catalysts.[12] Using *in situ* ATR-SEIRAS, the authors show that CO adsorption occurs between −0.1 V and 0.4 V *vs.* RHE as indicated by a rise in the intensity of a band from 2050 to 2100 cm^{-1}. At potentials more positive than 0.6 V, as the CO_{ads} band diminishes, a new band arises at 1460 cm^{-1} assigned to $CO_{3,ads}$ indicating that at more positive potentials, bicarbonate displaces CO_{ads} on the surface. At potentials more negative than −0.1 V, the adsorption of cations such as Na^+ (from the $NaHCO_3$ electrolyte), displace CO_{ads}. To observe the CO_2RR at potentials in which ATR-SEIRAS does not pick up CO_{ads} signals, they developed a potential step protocol where they alternate between reduction potentials at which the CO_2RR occurs and 0.4 V *vs.* RHE where the maximum CO_{ads} band intensity was observed. This allows for a fraction of CO produced to re-adsorb onto the Au electrode and therefore would be observable using ATR-SEIRAS. At potentials between −0.4 V and −0.6 V *vs.* RHE, the rate of CO production is significant as evidenced by a strong band at 2106 cm^{-1} which increased in intensity with decreasing potential.

Then, the authors utilized isotopic labeling coupled with the potential square-wave approach to gain insight into the mechanism of CO_2RR. The purge consisted of $^{13}CO_2$ while the electrolyte was comprised of 0.5 M $NaH^{12}CO_3$. They found that the unlabeled $^{12}CO_{ads}$ was observed initially, indicating that the carbon source is from the $H^{12}CO_3^-$ within the electrolyte and not the headspace $^{13}CO_2$ purge. In fact, utilizing a combination of MS and ATR-FTIR, they were able to determine that the composition of the dissolved CO_2 was 80% $^{12}CO_{2(aq)}$ matching closely with the isotopic composition of bicarbonate indicating a rapid equilibrium (faster than $CO_{2(g)}$ diffusion from the headspace) between $CO_{2(aq)}$ and bicarbonate (Fig. 9C). Further MS studies demonstrated that about 89% of the CO produced was ^{12}CO further demonstrating that the $CO_{2(aq)}$ equilibrated with bicarbonate is the major carbon source for the CO_2RR. Lastly, the authors conducted a kinetic analysis in which a bicarbonate first-order dependence was observed. The work describes the role of bicarbonate as a buffer as well as a $CO_{2(aq)}$ source leading to an increase in local $CO_{2(aq)}$ concentration and therefore enhancing the CO_2RR (Fig. 9D).

It is important to mention that, while water is an important source, the supporting electrolyte also contributes to the proton donation process in the CO_2RR. Resasco *et al.* found that the formation rates of H_2 and CH_4 strongly depend on the type and concentration of anions used.[96] The authors propose that this is due to the proton donating capability of certain anions whose pK_a is lower than water. Furthermore, a study conducted by Wuttig *et al.* found that the proton sources for CO_2RR on Au were bicarbonate, hydronium, and/or carbonic acid where the first electron transfer to form adsorbed H is rate limiting for H_2 evolution.[97]

Focused on a broader range of anions, Hong *et al.* studied the effects of anions such as Cl^-, HPO_4^{2-}, SO_4^{2-}, and HCO_3^- on the CO_2RR on Au sputtered gas diffusion electrode (Au/GDL) at a neutral pH.[95] The electrolyte containing Cl^- exhibited the highest CO FE out of all the other electrolytes reaching 82%, while the lowest CO FE was observed in electrolyte containing HPO_4^{2-} with 11%. The H_2 FE followed the opposite trend and the total current densities were similar, except for HPO_4^{2-}, whose H_2 FE was the highest with total current density nearly doubling indicating a substantial enhancement for HER. Structural characterizations ensured that the changes in CO_2RR activities in different electrolytes were due to the intrinsic properties of each anion. The authors propose that anion adsorption suppresses HER and promotes CO_2RR. Thus, higher CO_2RR activities are expected for anions with high binding strength to the surface. This idea explains the trend of increasing CO_2RR following: $Cl^- > SO_4^{2-} > HPO_4^{2-}$. However, a discrepancy in this theory was observed by the fact that HPO_4^{2-} binds more strongly than SO_4^{2-} and yet does not promote CO_2RR as much as SO_4^{2-}. The authors attribute this discrepancy to the intrinsic characteristics of HPO_4^{2-} and its ability to deprotonate further into PO_4^{3-} lowering the local pH and providing protons for the enhancement of the HER rather than the CO_2RR. Therefore, the authors claim that the identity of the anion is not the only factor that affects the CO_2RR but also its ability to deprotonate.

5. Summary and outlook

It is clear that electrochemical interfaces involve numerous components extending beyond the solid surface and its active sites in reactions like CO_2RR, HER/HOR, and OER/ORR. The growing interest in the role of interfacial liquids has led researchers to delve into their influence. These endeavors have provided insights into how these reactions truly unfold and can be enhanced at molecular levels. By deepening our understanding of these systems, we can explore strategies to manipulate interfacial liquids, thereby advancing existing technologies and fostering the development of new ones for a more sustainable future.

However, despite notable advancements in recent years, there remains much to unravel. Our current experimental methodologies face limitations in probing the constituents of the interfacial liquid and the electric double layer at high pre-

cision in terms of concentration, distribution, coordination, and orientation. Consequently, many mechanisms have primarily been explored through theoretical approaches. Yet, even in theory, the computational demands of considering the motions and interactions of all constituents simultaneously have led to simplified models that may lack comprehensiveness. Moreover, fully understanding the dynamic structure and properties of interfacial liquids proves challenging due to a lack of tools offering sufficient spatial and temporal resolution. These challenges have led to the formulation of various hypotheses to explain commonly observed effects or phenomena. Future research should prioritize the development of advanced experimental and theoretical methods that can thoroughly interrogate the intricacies of electrochemical interfaces, with a specific emphasis on the liquid phase. Additionally, the insights gleaned regarding interfacial liquid effects should be integral considerations in the design and application of catalyst materials for various electrochemical applications.

Author contributions

R. B. and D. K. conceptualized the manuscript. R. B., G. L., and D. K. wrote the original draft. R. B., G. L., and D. K. contributed to the revision of the manuscript. D. K. supervised the writing and revision of the manuscript, and provided the resources.

Conflicts of interest

The authors declare no competing interests.

Acknowledgements

The authors acknowledge the start-up support from the University of Pennsylvania as well as the generous support from Hanwha for this work.

References

1 P. C. K. Vesborg, B. Seger and I. Chorkendorff, *J. Phys. Chem. Lett.*, 2015, **6**, 951–957.
2 S. Bai, M. Yang, J. Jiang, X. He, J. Zou, Z. Xiong, G. Liao and S. Liu, *npj 2D Mater. Appl.*, 2021, **5**, 78.
3 J. Zhu, L. Hu, P. Zhao, L. Y. S. Lee and K.-Y. Wong, *Chem. Rev.*, 2020, **120**, 851–918.
4 Y. Lei, Z. Wang, A. Bao, X. Tang, X. Huang, H. Yi, S. Zhao, T. Sun, J. Wang and F. Gao, *Chem. Eng. J.*, 2023, **453**, 139663.
5 M. Shao, Q. Chang, J.-P. Dodelet and R. Chenitz, *Chem. Rev.*, 2016, **116**, 3594–3657.
6 S. Nitopi, E. Bertheussen, S. B. Scott, X. Liu, A. K. Engstfeld, S. Horch, B. Seger, I. E. L. Stephens, K. Chan, C. Hahn, J. K. Nørskov, T. F. Jaramillo and I. Chorkendorff, *Chem. Rev.*, 2019, **119**, 7610–7672.
7 D. Gao, R. M. Arán-Ais, H. S. Jeon and B. Roldan Cuenya, *Nat. Catal.*, 2019, **2**, 198–210.
8 B. M. Hunter, H. B. Gray and A. M. Müller, *Chem. Rev.*, 2016, **116**, 14120–14136.
9 M. M. Waegele, C. M. Gunathunge, J. Li and X. Li, *J. Chem. Phys.*, 2019, **151**, 160902.
10 L. Su, J. L. Weaver, M. Groenenboom, N. Nakamura, E. Rus, P. Anand, S. K. Jha, J. S. Okasinski, J. A. Dura and B. Reeja-Jayan, *ACS Appl. Mater. Interfaces*, 2021, **13**, 9919–9931.
11 X. Ding, D. Scieszka, S. Watzele, S. Xue, B. Garlyyev, R. W. Haid and A. S. Bandarenka, *ChemElectroChem*, 2022, **9**, e202101088.
12 M. Dunwell, Q. Lu, J. M. Heyes, J. Rosen, J. G. Chen, Y. Yan, F. Jiao and B. Xu, *J. Am. Chem. Soc.*, 2017, **139**, 3774–3783.
13 Y. Zheng, A. Vasileff, X. Zhou, Y. Jiao, M. Jaroniec and S.-Z. Qiao, *J. Am. Chem. Soc.*, 2019, **141**, 7646–7659.
14 R. Kortlever, J. Shen, K. J. P. Schouten, F. Calle-Vallejo and M. T. M. Koper, *J. Phys. Chem. Lett.*, 2015, **6**, 4073–4082.
15 L. R. L. Ting and B. S. Yeo, *Curr. Opin. Electrochem.*, 2018, **8**, 126–134.
16 N. Wang, S. Ma, P. Zuo, J. Duan and B. Hou, *Adv. Sci.*, 2021, **8**, 2100076.
17 L. Ge, H. Rabiee, M. Li, S. Subramanian, Y. Zheng, J. H. Lee, T. Burdyny and H. Wang, *Chem*, 2022, **8**, 663–692.
18 X. Tian, X. F. Lu, B. Y. Xia and X. W. Lou, *Joule*, 2020, **4**, 45–68.
19 A. Kulkarni, S. Siahrostami, A. Patel and J. K. Nørskov, *Chem. Rev.*, 2018, **118**, 2302–2312.
20 J. Song, C. Wei, Z.-F. Huang, C. Liu, L. Zeng, X. Wang and Z. J. Xu, *Chem. Soc. Rev.*, 2020, **49**, 2196–2214.
21 A. Raveendran, M. Chandran and R. Dhanusuraman, *RSC Adv.*, 2023, **13**, 3843–3876.
22 A. C. Garcia, T. Touzalin, C. Nieuwland, N. Perini and M. T. M. Koper, *Angew. Chem., Int. Ed.*, 2019, **58**, 12999–13003.
23 R. R. Rao, B. Huang, Y. Katayama, J. Hwang, T. Kawaguchi, J. R. Lunger, J. Peng, Y. Zhang, A. Morinaga, H. Zhou, H. You and Y. Shao-Horn, *J. Phys. Chem. C*, 2021, **125**, 8195–8207.
24 M. C. O. Monteiro, F. Dattila, N. López and M. T. M. Koper, *J. Am. Chem. Soc.*, 2022, **144**, 1589–1602.
25 S. Hou, L. Xu, X. Ding, R. M. Kluge, T. K. Sarpey, R. W. Haid, B. Garlyyev, S. Mukherjee, J. Warnan, M. Koch, S. Zhang, W. Li, A. S. Bandarenka and R. A. Fischer, *Angew. Chem., Int. Ed.*, 2022, **61**, e202201610.
26 K. Holst-Olesen, M. Reda, H. A. Hansen, T. Vegge and M. Arenz, *ACS Catal.*, 2018, **8**, 7104–7112.
27 V. R. Stamenkovic, D. Strmcnik, P. P. Lopes and N. M. Markovic, *Nat. Mater.*, 2017, **16**, 57–69.
28 H. Khani, A. R. Puente Santiago and T. He, *Angew. Chem., Int. Ed.*, 2023, e202306103.
29 B. Deng, M. Huang, X. Zhao, S. Mou and F. Dong, *ACS Catal.*, 2022, **12**, 331–362.
30 Y. J. Sa, C. W. Lee, S. Y. Lee, J. Na, U. Lee and Y. J. Hwang, *Chem. Soc. Rev.*, 2020, **49**, 6632–6665.

31 X. Lu, W. Tu, Y. Zhou and Z. Zou, *Adv. Energy Mater.*, 2023, **13**, 2300628.
32 C. Cheng, M. Deng, L. Li and Z. Wei, *Sci. China: Chem.*, 2022, **65**, 1854–1866.
33 I. Ledezma-Yanez, W. D. Z. Wallace, P. Sebastián-Pascual, V. Climent, J. M. Feliu and M. T. M. Koper, *Nat. Energy*, 2017, **2**, 17031.
34 P. Li, Y. Jiang, Y. Hu, Y. Men, Y. Liu, W. Cai and S. Chen, *Nat. Catal.*, 2022, **5**, 900–911.
35 K. Zhao, X. Chang, H.-S. Su, Y. Nie, Q. Lu and B. Xu, *Angew. Chem., Int. Ed.*, 2022, **61**, e202207197.
36 S. Intikhab, L. Rebollar, Y. Li, R. Pai, V. Kalra, M. H. Tang and J. D. Snyder, *ACS Catal.*, 2020, **10**, 6798–6802.
37 L. Rebollar, S. Intikhab, S. Zhang, H. Deng, Z. Zeng, J. D. Snyder and M. H. Tang, *J. Catal.*, 2021, **398**, 161–170.
38 Y.-H. Wang, S. Zheng, W.-M. Yang, R.-Y. Zhou, Q.-F. He, P. Radjenovic, J.-C. Dong, S. Li, J. Zheng, Z.-L. Yang, G. Attard, F. Pan, Z.-Q. Tian and J.-F. Li, *Nature*, 2021, **600**, 81–85.
39 Q. Sun, N. J. Oliveira, S. Kwon, S. Tyukhtenko, J. J. Guo, N. Myrthil, S. A. Lopez, I. Kendrick, S. Mukerjee, L. Ma, S. N. Ehrlich, J. Li, W. A. Goddard, Y. Yan and Q. Jia, *Nat. Energy*, 2023, **8**, 859–869.
40 K. Lourenssen, J. Williams, F. Ahmadpour, R. Clemmer and S. Tasnim, *J. Energy Storage*, 2019, **25**, 100844.
41 S. N. Suarez, J. R. Jayakody, S. G. Greenbaum, T. Zawodzinski Jr. and J. J. Fontanella, *J. Phys. Chem. B*, 2010, **114**, 8941–8947.
42 L. Su, J. Chen, F. Yang, P. Li, Y. Jin, W. Luo and S. Chen, *J. Am. Chem. Soc.*, 2023, **145**, 12051–12058.
43 S. Sharifi Golru and E. J. Biddinger, *Chem. Eng. J.*, 2022, **428**, 131303.
44 N. Mohandas, T. N. Narayanan and A. Cuesta, *ACS Catal.*, 2023, **13**, 8384–8393.
45 B. Yang, H. Lang, Z. Liu, S. Wang, Z. Men and C. Sun, *J. Mol. Liq.*, 2021, **324**, 114996.
46 Y. Meng, Z. Xu, Z. Shen, Q. Xia, Y. Cao, Y. Wang and X. Li, *J. Mater. Chem. A*, 2022, **10**, 6508–6522.
47 W. Ge, Y. Chen, Y. Fan, Y. Zhu, H. Liu, L. Song, Z. Liu, C. Lian, H. Jiang and C. Li, *J. Am. Chem. Soc.*, 2022, **144**, 6613–6622.
48 B. Huang, R. R. Rao, S. You, K. Hpone Myint, Y. Song, Y. Wang, W. Ding, L. Giordano, Y. Zhang, T. Wang, S. Muy, Y. Katayama, J. C. Grossman, A. P. Willard, K. Xu, Y. Jiang and Y. Shao-Horn, *JACS Au*, 2021, **1**, 1674–1687.
49 S. Xue, B. Garlyyev, S. Watzele, Y. Liang, J. Fichtner, M. D. Pohl and A. S. Bandarenka, *ChemElectroChem*, 2018, **5**, 2326–2329.
50 Y. Taji, A. Zagalskaya, I. Evazzade, S. Watzele, K.-T. Song, S. Xue, C. Schott, B. Garlyyev, V. Alexandrov, E. Gubanova and A. S. Bandarenka, *Nano Mater. Sci.*, 2022, DOI: **10.1016/j.nanoms.2022.09.003**.
51 J. T. Bender, A. S. Petersen, F. C. Østergaard, M. A. Wood, S. M. J. Heffernan, D. J. Milliron, J. Rossmeisl and J. Resasco, *ACS Energy Lett.*, 2023, **8**, 657–665.
52 L. Jiao, E. Liu, S. Mukerjee and Q. Jia, *ACS Catal.*, 2020, **10**, 11099–11109.
53 A. Goyal and M. T. M. Koper, *Angew. Chem., Int. Ed.*, 2021, **60**, 13452–13462.
54 M. C. O. Monteiro, A. Goyal, P. Moerland and M. T. M. Koper, *ACS Catal.*, 2021, **11**, 14328–14335.
55 A. H. Shah, Z. Zhang, Z. Huang, S. Wang, G. Zhong, C. Wan, A. N. Alexandrova, Y. Huang and X. Duan, *Nat. Catal.*, 2022, **5**, 923–933.
56 X. Chen, I. T. McCrum, K. A. Schwarz, M. J. Janik and M. T. M. Koper, *Angew. Chem., Int. Ed.*, 2017, **56**, 15025–15029.
57 N. Perini and E. A. Ticianelli, *J. Catal.*, 2019, **378**, 277–282.
58 A. M. Raventos and R. Kortlever, *Electrochim. Acta*, 2022, **415**, 140255.
59 R. A. Márquez, K. Kawashima, Y. J. Son, G. Castelino, N. Miller, L. A. Smith, C. E. Chukwuneke and C. B. Mullins, *ACS Energy Lett.*, 2023, **8**, 1141–1146.
60 T. Kumeda, H. Tajiri, O. Sakata, N. Hoshi and M. Nakamura, *Nat. Commun.*, 2018, **9**, 4378.
61 M. Görlin, J. Halldin Stenlid, S. Koroidov, H.-Y. Wang, M. Börner, M. Shipilin, A. Kalinko, V. Murzin, O. V. Safonova, M. Nachtegaal, A. Uheida, J. Dutta, M. Bauer, A. Nilsson and O. Diaz-Morales, *Nat. Commun.*, 2020, **11**, 6181.
62 J. D. Michael, E. L. Demeter, S. M. Illes, Q. Fan, J. R. Boes and J. R. Kitchin, *J. Phys. Chem. C*, 2015, **119**, 11475–11481.
63 B. Garlyyev, S. Xue, M. D. Pohl, D. Reinisch and A. S. Bandarenka, *ACS Omega*, 2018, **3**, 15325–15331.
64 D. Strmcnik, K. Kodama, D. van der Vliet, J. Greeley, V. R. Stamenkovic and N. M. Marković, *Nat. Chem.*, 2009, **1**, 466–472.
65 M. C. O. Monteiro, F. Dattila, B. Hagedoorn, R. García-Muelas, N. López and M. T. M. Koper, *Nat. Catal.*, 2021, **4**, 654–662.
66 V. J. Ovalle, Y.-S. Hsu, N. Agrawal, M. J. Janik and M. M. Waegele, *Nat. Catal.*, 2022, **5**, 624–632.
67 J. Resasco, L. D. Chen, E. Clark, C. Tsai, C. Hahn, T. F. Jaramillo, K. Chan and A. T. Bell, *J. Am. Chem. Soc.*, 2017, **139**, 11277–11287.
68 J. Gu, S. Liu, W. Ni, W. Ren, S. Haussener and X. Hu, *Nat. Catal.*, 2022, **5**, 268–276.
69 S. Ringe, E. L. Clark, J. Resasco, A. Walton, B. Seger, A. T. Bell and K. Chan, *Energy Environ. Sci.*, 2019, **12**, 3001–3014.
70 X. Qin, T. Vegge and H. A. Hansen, *J. Am. Chem. Soc.*, 2023, **145**, 1897–1905.
71 S.-J. Shin, H. Choi, S. Ringe, D. H. Won, H.-S. Oh, D. H. Kim, T. Lee, D.-H. Nam, H. Kim and C. H. Choi, *Nat. Commun.*, 2022, **13**, 5482.
72 G. Kastlunger, L. Wang, N. Govindarajan, H. H. Heenen, S. Ringe, T. Jaramillo, C. Hahn and K. Chan, *ACS Catal.*, 2022, **12**, 4344–4357.
73 D. Kim, S. Yu, F. Zheng, I. Roh, Y. Li, S. Louisia, Z. Qi, G. A. Somorjai, H. Frei, L.-W. Wang and P. Yang, *Nat. Energy*, 2020, **5**, 1032–1042.
74 M. R. Singh, Y. Kwon, Y. Lum, J. W. Ager III and A. T. Bell, *J. Am. Chem. Soc.*, 2016, **138**, 13006–13012.

75 O. Ayemoba and A. Cuesta, *ACS Appl. Mater. Interfaces*, 2017, **9**, 27377–27382.
76 F. Zhang and A. C. Co, *Angew. Chem., Int. Ed.*, 2020, **59**, 1674–1681.
77 Y.-Q. Wang, X.-H. Dan, X. Wang, Z.-Y. Yi, J. Fu, Y.-C. Feng, J.-S. Hu, D. Wang and L.-J. Wan, *J. Am. Chem. Soc.*, 2022, **144**, 20126–20133.
78 E. Pérez-Gallent, G. Marcandalli, M. C. Figueiredo, F. Calle-Vallejo and M. T. M. Koper, *J. Am. Chem. Soc.*, 2017, **139**, 16412–16419.
79 A. S. Malkani, J. Li, N. J. Oliveira, M. He, X. Chang, B. Xu and Q. Lu, *Sci. Adv.*, 2020, **6**, eabd2569.
80 D. V. Tripkovic, D. Strmcnik, D. van der Vliet, V. Stamenkovic and N. M. Markovic, *Faraday Discuss.*, 2009, **140**, 25–40.
81 E. Lamy-Pitara, S. El Mouahid and J. Barbier, *Electrochim. Acta*, 2000, **45**, 4299–4308.
82 G. A. Kamat, J. A. Zamora Zeledón, G. T. K. K. Gunasooriya, S. M. Dull, J. T. Perryman, J. K. Nørskov, M. B. Stevens and T. F. Jaramillo, *Commun. Chem.*, 2022, **5**, 20.
83 J. A. Z. Zeledón, G. A. Kamat, G. T. K. K. Gunasooriya, J. K. Nørskov, M. B. Stevens and T. F. Jaramillo, *ChemElectroChem*, 2021, **8**, 2467–2478.
84 F. Zhou, Y. Yan, S. Guan, W. Guo, M. Sun and M. Pan, *Int. J. Energy Res.*, 2020, **44**, 10155–10167.
85 G. You, W. Zhu and Z. Zhuang, *Int. J. Hydrogen Energy*, 2019, **44**, 13373–13382.
86 Z. Jusys and R. J. Behm, *ChemPhysChem*, 2019, **20**, 3276–3288.
87 M. Luo and M. T. M. Koper, *Nat. Catal.*, 2022, **5**, 615–623.
88 A. S. Varela, W. Ju, T. Reier and P. Strasser, *ACS Catal.*, 2016, **6**, 2136–2144.
89 Y. Zhang, L. Liu, L. Shi, T. Yang, D. Niu, S. Hu and X. Zhang, *Electrochim. Acta*, 2019, **313**, 561–569.
90 T. Yuan, T. Wang, G. Zhang, W. Deng, D. Cheng, H. Gao, J. Zhao, J. Yu, P. Zhang and J. Gong, *Chem. Sci.*, 2022, **13**, 8117–8123.
91 H. Wang, E. Matios, C. Wang, J. Luo, X. Lu, X. Hu and W. Li, *Nano Lett.*, 2019, **19**, 3925–3932.
92 M. G. Kibria, C.-T. Dinh, A. Seifitokaldani, P. De Luna, T. Burdyny, R. Quintero-Bermudez, M. B. Ross, O. S. Bushuyev, F. P. García de Arquer, P. Yang, D. Sinton and E. H. Sargent, *Adv. Mater.*, 2018, **30**, 1804867.
93 I. T. McCrum, S. A. Akhade and M. J. Janik, *Electrochim. Acta*, 2015, **173**, 302–309.
94 Y. Huang, C. W. Ong and B. S. Yeo, *ChemSusChem*, 2018, **11**, 3299–3306.
95 S. Hong, S. Lee, S. Kim, J. K. Lee and J. Lee, *Catal. Today*, 2017, **295**, 82–88.
96 J. Resasco, Y. Lum, E. Clark, J. Z. Zeledon and A. T. Bell, *ChemElectroChem*, 2018, **5**, 1064–1072.
97 A. Wuttig, M. Yaguchi, K. Motobayashi, M. Osawa and Y. Surendranath, *Proc. Natl. Acad. Sci. U. S. A.*, 2016, **113**, E4585–E4593.